

UNCLASSIFIED

| |
|--|
| |
| |
| |
| |
| AD NUMBER |
| AD866080 |
| NEW LIMITATION CHANGE |
| TO Approved for public release, distribution unlimited |
| FROM Distribution authorized to U.S. Gov't. agencies and their contractors; Administrative/Operational Use; JAN 1970. Other requests shall be referred to Air Force Materials Lab., AFSC, Wright-Patterson AFB, OH 45433. |
| AUTHORITY |
| AFML ltr, 12 Jan 1972 |

THIS PAGE IS UNCLASSIFIED

AD 866080

AFML-TR-67-143
PART III

ELASTIC-PLASTIC FRACTURE MECHANICS

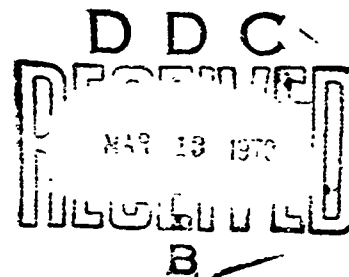
G. T. HAHN, A. R. ROSENFELD, and M. SARRATE

Battelle Memorial Institute

Columbus Laboratories

TECHNICAL REPORT AFML-TR-67-143, PART III

JANUARY 1970



This document is subject to special export controls and each transmittal to foreign governments or foreign nationals may be made only with prior approval of the Metals and Ceramics Division (MAM), Air Force Materials Laboratory, Wright-Patterson Air Force Base, Ohio 45433.

AIR FORCE MATERIALS LABORATORY
AIR FORCE SYSTEMS COMMAND
WRIGHT-PATTERSON AIR FORCE BASE, OHIO

Reproduced by the
CLEARINGHOUSE
for Federal Scientific & Technical
Information Springfield Va 22151

NOTICE

When Government drawings, specifications, or other data are used for any purpose other than in connection with a definitely related Government procurement operation, the United States Government thereby incurs no responsibility nor any obligation whatsoever; and the fact that the Government may have formulated furnished, or in any way supplied the said drawings, specifications, or other data is not to be regarded by implication or otherwise as in any manner licensing the holder or any other person or corporation, or conveying any rights or permission to manufacture, use, or sell any patented invention that may in any way be related thereto.

This document is subject to special export controls and each transmittal to foreign governments or foreign nationals may be made only with prior approval of the Metals and Ceramics Division (MAM), Air Force Materials Laboratory, Wright-Patterson Air Force Base, Ohio 45433.

The distribution of this report is limited to protect technical information relating to technology restricted by U.S. Export Control Act.

| | |
|---------------------------------|-----------------------|
| ACCOMPLISHMENT | |
| OFFICE | WHITE SECTION 1 |
| CODE | BLUE SECTION 1 |
| DATE | |
| BY | |
| DISTRIBUTION/AVAILABILITY CODES | |
| DISC. | AVAIL. and/or SPECIAL |

Copies of this report should not be returned unless return is required by security considerations, contractual obligations, or notice on a specific document.

ELASTIC-PLASTIC FRACTURE MECHANICS

G. T. HAHN, A. R. ROSENFELD, and M. SARRATE*

This document is subject to special export controls and each transmittal to foreign governments or foreign nationals may be made only with prior approval of the Metals and Ceramics Division (MAM), Air Force Materials Laboratory, Wright-Patterson Air Force Base, Ohio 45433.

*M. Sarrate was on leave of absence from the Argentine Atomic Energy Commission.


FOREWORD

This report was prepared by personnel of the Columbus Laboratories of Battelle Memorial Institute under USAF Contract No. AF 33(615)-3565. The contract was initiated under Project No. 7351, "Metallic Materials", Task No. 735106, "Behavior of Metals". The contract was administered under the direction of the Metals and Ceramics Division of the Air Force Materials Laboratory, Wright-Patterson Air Force Base, with Mr. A. W. Brisbane acting as project engineer.

The authors are grateful to W. J. Trapp, A. W. Brisbane and F. Ostermann for their encouragement and support of this work. They are indebted to H. Mindlin for assistance in conducting the fatigue tests, P. Mincer for the metallographic work and to C. Pepper for her work on the manuscript. They also wish to thank C. Laird, R. Hoagland, and J. Barsom for stimulating and useful discussions.

The work reported began on 1 April 1968, and was concluded on 30 September 1969. This report was submitted by the authors 30 September, 1969.

This technical report has been reviewed and is approved.



W. J. TRAPP
Chief, Strength and Dynamics Branch
Metals and Ceramics Division
Air Force Materials Laboratory

ABSTRACT

This report describes experiments that delineate the plastic zone of a growing fatigue crack and its relation to the zone of a monotonically loaded, stationary crack. A compilation of cyclic crack growth measurements is also presented. Preliminary results of the zone studies and the data compilation are examined with respect to the mechanism of cyclic growth and the contribution of metallurgical factors.

Two techniques, etch pitting and interferometry, are used to reveal the plastic zones produced by growing fatigue cracks in Fe-3Si Steel (under plane strain) and in cold worked steel (under plane stress), respectively. In addition, a method of simulating cyclic crack growth under controlled conditions by cutting-in slits under load with intermittent load reversals is demonstrated. The preliminary results indicate that the plastic deformation generated by each loading cycle is similar to the deformation of the monotonic zone.

The results provide a basis for extending numerical treatments of the monotonically loaded crack to the fatigue crack problem. Estimates are made in this way of the number of plastic strain cycles experienced by the material in front of a growing fatigue crack and also the crack-tip displacement. These values together with the compilation of crack growth measurements are examined in the light of two fatigue crack growth mechanisms: (1) irreversible crack blunting, and (2) Manson-Coffin type strain accumulation. This shows that both mechanisms can account for the value of the stress intensity exponent, $m \approx 2$ observed in Regime No. 1 (the high cycle-low stress portion of the crack growth spectrum). While neither mechanism easily accounts for the invariance of crack growth rates in Regime No. 2, the existing observations are more easily rationalized in terms of blunting. A possible explanation for the greater stress sensitivity and higher growth rates in Regime No. 2 is offered in terms of an increasing length of active crack front.

Both the theoretical treatment and the bulk of the test data show that the resistance to fatigue crack growth in Regime No. 1 is relatively insensitive to composition and metallurgical structure, provided environmental effects are not involved. In contrast, significant improvements in fatigue life could be achieved simply by postponing the onset of Regime No. 2, a feature that should depend on metallurgical variables.

This abstract is subject to special export controls and each transmittal to foreign governments or foreign nationals may be made only with prior approval of the Metals and Ceramics Division (MAMD), Air Force Materials Laboratory, Wright-Patterson Air Force Base, Ohio 45433.

TABLE OF CONTENTS

| | <u>Page</u> |
|---|-------------|
| I. EXPERIMENTS ON THE NATURE OF THE FATIGUE CRACK PLASTIC ZONE | 1 |
| INTRODUCTION | 1 |
| EXPERIMENTAL PROCEDURE | 2 |
| Plane Stress | 2 |
| Plane Strain | 2 |
| RESULTS | 4 |
| Plane Stress | 4 |
| Plane Strain | 10 |
| DISCUSSION | 29 |
| CONCLUSIONS | 39 |
| REFERENCES | 40 |
| II. APPENDIX A--Compilation of Cyclic Crack-Growth Rate Measurements | 45 |
| APPENDIX B--Simplified Formulations of the Cyclic Crack Growth Mechanisms | 49 |
| APPENDIX C--Augmented Dugdale Model | 50 |

LIST OF ILLUSTRATIONS

Figure

| | | |
|---|---|----|
| 1 | Cantilever Fracture Toughness Specimen | 3 |
| 2 | Stress-Strain Characteristics of the Fe-3Si Steel at 100 C | 3 |
| 3 | Strain Distribution Ahead of a Slit Revealed Under Load by Interferometric Fringe Pattern | 5 |
| 4 | Influence of Cyclic Loading, $\frac{\Delta K}{\sigma_Y} = 0.225 \sqrt{\text{in}}$, ON THE STEEL FOIL . . | 7 |
| 5 | Influence of Cyclic Loading on the Crack Tip ϵ_z -STRAIN PROFILES | 8 |
| 6 | Plastic Zone Produced in the Interior of Specimen 3P-20 By the Fatigue Simulation Procedure | 11 |

LIST OF ILLUSTRATIONS (Continued)

| <u>Figure</u> | <u>Page</u> |
|---|-------------|
| 7 Plastic Zone Produced in the Interior of Specimen 3P-19 By Monotonic Loading Simulation | 13 |
| 8 Plastic Zone Produced in the Interior of Specimen 3P-18 By the Stable Growth Simulation Procedure | 15 |
| 9 Plastic Zone of a Mixed Fatigue-Cleavage Crack Produced In Specimen 3P-24 By 21,770 Cycles with a Stress Intensity Range $\frac{\Delta K}{\sigma_Y} = 0.7 \sqrt{\text{in}}$ | 18 |
| 10 Plastic Zone of a Mixed Fatigue-Cleavage Crack Produced in Specimen 3P-25 By 9930 Cycles with a Stress Intensity Range $\frac{\Delta K}{\sigma_Y} = 0.7 \sqrt{\text{in}}$ | 24 |
| 11 Comparison of Fatigue Crack- and Stationary, Virgin Crack-Near- Tip Zones | 28 |
| 12 Schematic of Monotonically Loaded Crack Tip Plastic Zone | 31 |
| 13 Simplified Schematic Representation of the Origin of Regimes No. 1 and No. 2 | 38 |
| A-1 Schematic of Stress-Intensity-Growth Rate Spectrum with 2 Regimes and Definitions of Terms in Table A-1 | 48 |
| C-1 Augmented Dugdale Crack Model | 51 |

LIST OF TABLES

| <u>Table</u> | |
|--|----|
| 1 Summary of COD and Crack-Tip Strain Values | 9 |
| 2 Summary of Plastic Zone Size-Values Obtained from Etching Experiments | 17 |
| 3 Estimates of η and η' , the Numbers of Plastic Strain Cycles and β , the Ratio of Crack Growth Per Cycle to Crack-Opening Displacement | 32 |
| 4 Summary of Selected Cyclic Crack Growth Resistance Values | 35 |
| A-1 Summary of Cyclic Crack Growth Data | 46 |

EXPERIMENTS ON THE NATURE OF THE FATIGUE CRACK PLASTIC ZONE

INTRODUCTION

Until recently, few generalizations could be made about fatigue crack growth. Although much of the data has been expressed as a power relation†: $\frac{da}{dN} = A(\Delta K)^m$, neither of the curve-fitting parameters is, in general, a constant. Both m , and A depend on the stress range, the material, the test environment, and the exact details of the testing procedure. In the absence of correlations, it has been difficult to identify the metallurgical influences on the fatigue crack growth resistance.

Now, with the accumulation of more test data, (1-27) patterns are beginning to emerge. The compilation in Appendix A contains evidence of two growth-rate regimes within which many alloys display striking similarities. Progress is also being made on the analytical front; see Rice⁽²⁸⁾ for a comprehensive review and more recent treatments by Rice and Johnson⁽²⁹⁾, Erdogan⁽³⁰⁾, and Liu and co-workers^(22,31). These analyses hinge on the two mechanisms of crack advance that have been proposed: (1) irreversible plastic blunting⁽³²⁻³⁴⁾ and (2) Manson⁽³⁵⁾-Coffin⁽³⁶⁾-type damage accumulation. They also depend on descriptions of the strain distribution in the locale of the fatigue crack^(34,37,38).

The experimental work described in this report deals with the plastic zone of a growing fatigue crack and its relation to the zone of a monotonically loaded, stationary crack. This subject is virtually unexplored because of the experimental difficulties, and only one set of measurements, by Liu and Iino⁽²²⁾ are known to the authors. The present study examines ways of applying two techniques: etch pitting and interferometry, to reveal the plastic zones produced by fatigue cracks under plane strain and plane stress conditions. Preliminary results are reported and these indicate that the plastic deformation generated by each loading cycle is similar to the zone of a stationary crack loaded monotonically.

On this basis, theoretical treatments of the monotonically loaded crack are tentatively extended to the fatigue crack problem. Simplified formulations of the plastic blunting and damage accumulation are obtained in this way. The efficiency of the blunting mechanism and the number of plastic strain cycles experienced by material in front of the crack is estimated. This shows that both mechanisms can account for the value of the stress intensity exponent, $m \approx 2$ observed in Regime No. 1 (the high cycle-low stress portion of the crack growth spectrum). While neither mechanism easily accounts for the invariance of crack growth rates in Regime No. 1, the existing observations are more easily ration-

† $\frac{da}{dN}$ is the cyclic crack growth rate, ΔK is the cyclic stress intensity variation, A is a materials parameter and m is a numerical constant.

alized in terms of blunting. A possible explanation is offered for the higher m -values and growth rates of Regime No. 2 (the low cycle-high stress range). Implications with respect to the metallurgical origins of the cyclic crack growth resistance and the prospects of improving it are discussed.

EXPERIMENTAL PROCEDURE

Plane Stress

Plastic zones under plane stress were revealed in an 0.00175 in. thick, cold rolled, mild steel foil--yield strength: 105,000 psi and toughness: $K_{IC} = 34 \text{ ksi}\sqrt{\text{in}}$ --whose fracture behavior has been reported on before (39-40). The behavior of the foil approximates two idealizations: elastic-perfectly plastic behavior and plane stress deformation. Because plane stress conditions are approached, the deformation within the plastic zone ahead of a crack is mainly transverse to the surface and easily measured.

The foil specimen was 4.0" long by 3.9" wide with a centrally located notch 0.220" long cut in by spark machining. It was prepolished to give a smooth surface and mounted in a small tensioning device which could be placed on the stage of an interference microscope. The strain distribution could thus be detected under load as well as after unloading. The specimen was loaded by means of a screw-and-lever arrangement, the load being monitored with an electric resistance strain gage (more detailed descriptions of the experimental methods are given in References (39) and (40)). The fatigue loading corresponds to cycling between stress-intensity levels of $K/\sigma_Y = 0.025$ - $0.25\sqrt{\text{in}}$. After varying numbers of cycles, the loading was interrupted and interference patterns of the strain distribution at maximum and minimum loads were made.

Plane Strain

Studies of plastic zones under plane strain employed 1/2 in.-thick, Fe-3Si steel plates as the model material[†]. Descriptions of the material and the procedure for revealing zones on the surface and on interior sections by etching, as well as the zones displayed by virgin, stationary cracks in this steel after one cycle load-unload are given in Reference (41). Unlike the earlier work, the present studies were conducted with the DCB (double cantilever beam) specimen shown in Figure 1. Stress intensity values were calculated from the Mostovoy relation⁽⁴²⁾ and checked against compliance measurements. In an effort to avoid cleavage, the tests were carried out at 100 C, but this strategy was only partially successful. Cleavage can probably be avoided in future experiments by lowering the silicon content. The tensile properties of the steel at 100 C, in Figure 2, show that the yield stress is 54,000 psi at this temperature.

In the first experiment fatigue crack growth was simulated by cutting in a sharp slit under load with intermittent unloading. The specimen was first

[†] Nominal Composition Si: 3.4%, C: 0.02% remainder Fe.

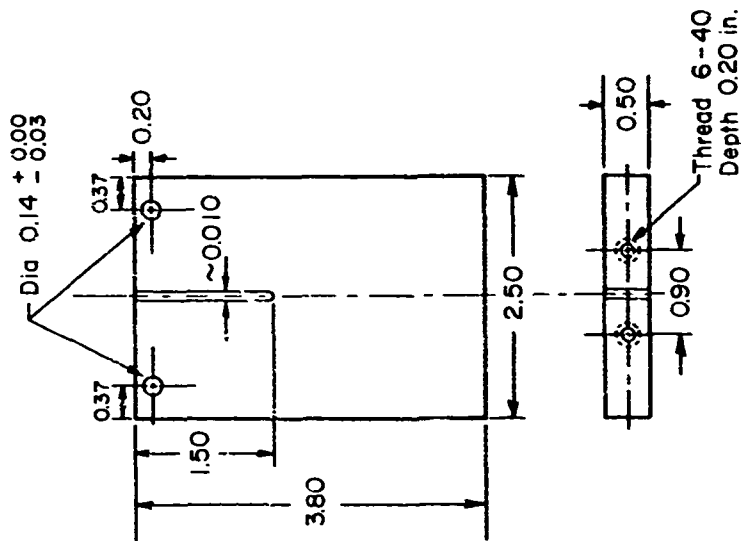


FIGURE 1. CANTILEVER FRACTURE TOUGHNESS SPECIMEN

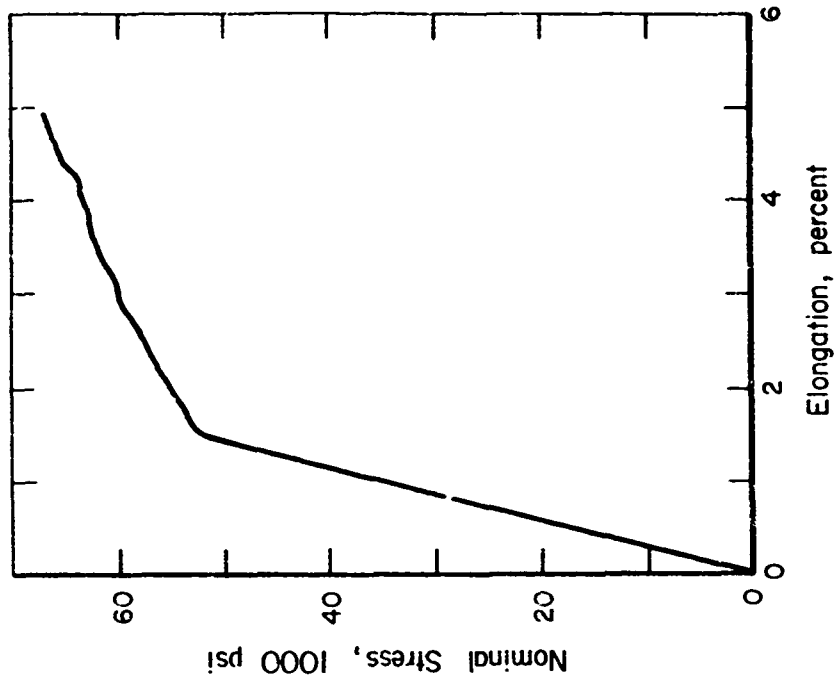


FIGURE 2. STRESS-STRAIN CHARACTERISTICS OF THE Fe-3Si STEEL AT 100 C

loaded to a predetermined stress intensity level, $\frac{K}{\sigma_Y} = 0.7 \sqrt{\text{in}}$ † in a horizontal tensile testing machine. Then the slit was extended 0.0008 in. by spark machining†† under load. At this point, the specimen was unloaded, and reloaded to $\frac{K}{\sigma_Y} = 0.7 \sqrt{\text{in}}$, and the sequence of steps, cutting, unloading, and reloading 50 times in quick succession. Effects of the stress reversals within zone and the plastic region left behind the growing slit were discerned by comparisons with the zones produced by:

- (i) A virgin slit subjected to one cycle of loading, and by
- (ii) A slit cut in under load with the load controlled to produce a constant stress intensity at the crack tip which are described more fully elsewhere.⁽⁴³⁾

In the second type of experiment, actual fatigue cracks were generated in pre-slitted DCB specimens and grown by cycling between a small preload and a maximum load and deflection controlled to give a fixed stress intensity range of $\frac{\Delta K}{\sigma_Y} = 0.7 \sqrt{\text{in}}$. These experiments were performed at 10 cps in a standard hydraulic fatigue testing machine. The zones associated with these cracks were then revealed by etching.

RESULTS

Plane Stress

Figure 3 illustrates the condition of a sample under load after the first 1/2 fatigue cycle and the information derived from the interferometric fringe pattern (Figure 3a)†††. No crack growth was discernible in the steel foil after

† K is the stress intensity, and σ_Y is the yield stress.

†† The slits were spark machined with a 0.005 in. diameter copper wire which produces a slit ~ 0.010 in. wide with a ~ 0.005 in. root radius.

††† The pattern reflects the distribution of the through-the-thickness strain ϵ_z , and this can be converted into an isostrain contour map (Figure 3b) which shows the general shape of the zone, the zone length and the zone width at the crack (or slit) tip, as well as the distribution of strain within. Since the patterns are difficult to interpret right at the crack (or slit) tip, values attributed to the crack tip, i.e. at $x = c$, were always measured 0.001 in. from the tip. The ϵ_z -profile at a particular distance from the crack tip can also be constructed (Figure 3c). The peak strain displayed by the profile at the crack tip, $x = c$, is referred to here as the crack-tip strain or ϵ_c . The area within this profile, i.e., $-2 \int_0^c \epsilon_z dY$ represents the COD, or crack opening displacement. The fact that the zones are necked largely precludes in-plane strain: $\epsilon_x = 0$. This and the constancy of volume give the result: $\epsilon_Y = -\epsilon_z$ (see Figure 4b for coordinates). Consequently, the COD (the total Y-displacement at the crack tip arising from plastic deformation) is: $\text{COD} = 2 \int \epsilon_Y dY = -2 \int \epsilon_z dY$. Note that the zone in Figure 3 represents the deformation produced by the first half of a single load-unload cycle involving a stress intensity range $\frac{\Delta K}{\sigma_Y} = 0.3 \sqrt{\text{in}}$, the zone corresponding to the first half of the cycle employed in the fatigue experiments $\frac{\Delta K}{\sigma_Y} = 0.25 \sqrt{\text{in}}$ was similar in character but about 15% smaller.

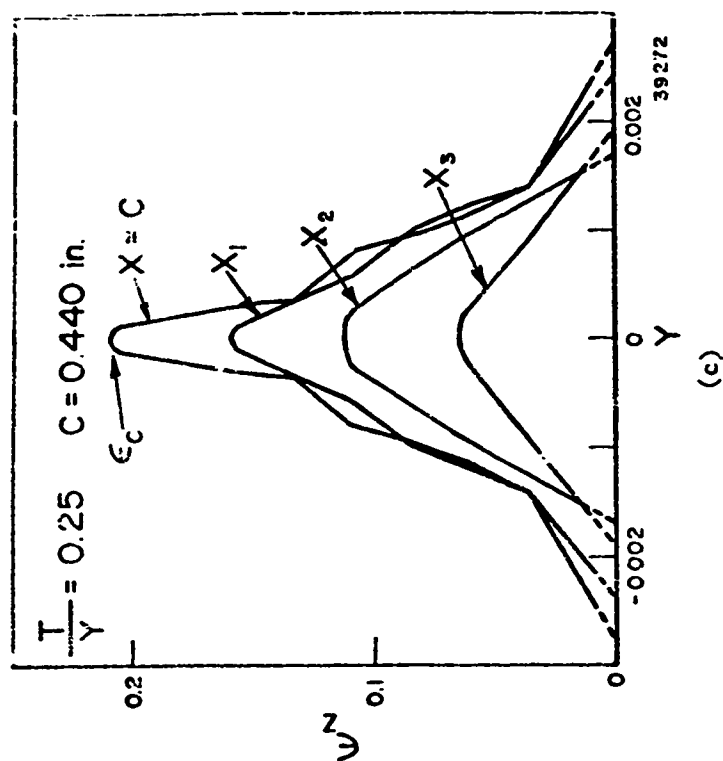
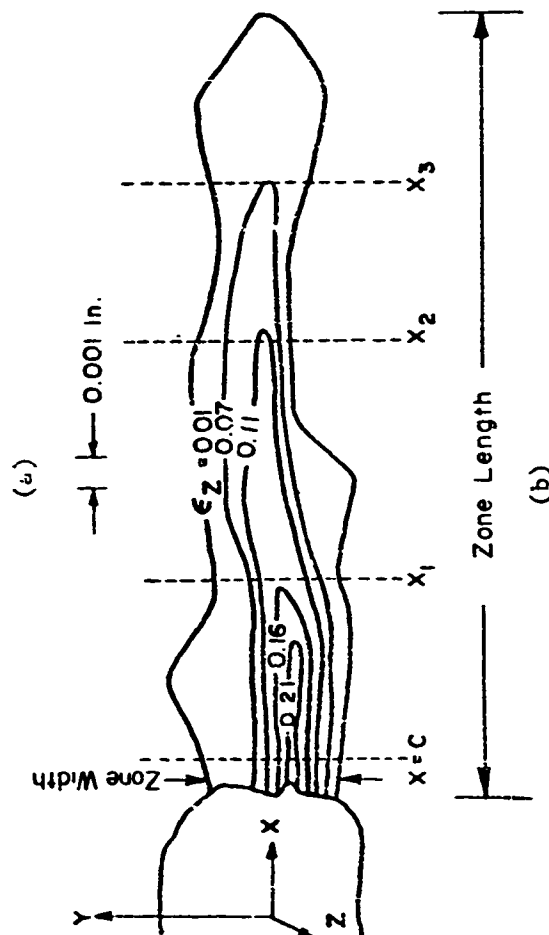
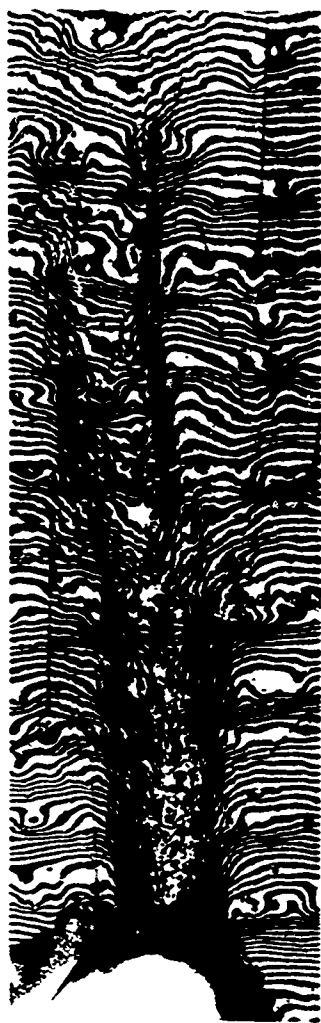


FIGURE 3. STRAIN DISTRIBUTION AHEAD OF A SLIT REVEALED UNDER LOAD BY INTERFEROMETRIC FRINGE PATTERN: (a) fringe pattern displayed by sample with $c = 0.440$ in. loaded to $T/Y = 0.25$, $K/Y = 0.30 \sqrt{\text{in.}}$, (b) the isostrain contours derived from the fringes, and (c) the ϵ_z -strain profile at four points along the plastic zone. (a) and (b) 150X

the ten cycles of loading, but when the fatiguing was interrupted for zone measurement after twenty cycles the crack had extended slightly at either end (Figure 4a). Eventually, the growth rate settled down to a roughly constant value of $\sim 2 \times 10^{-4}$ in/cycle.^{††} This rate is not unlike those reported for high strength structural alloys at comparable $\frac{\Delta K}{\sigma_Y}$ - levels. It also appears that the initial growth rate is slightly larger than during steady-state growth.

Qualitatively, the plastic zone had the same long, narrow shape after many cycles of loading as it did after the first cycle before crack growth was observed. Both the zone length and the zone width increase as a result of cyclic loading. The zone length after one cycle is within the range (but somewhat on the high side) of our previous measurements. During the first few cycles of loading, the length remains roughly constant and only appears to increase upon the onset of crack growth (Figure 4b). During crack growth, the length again remains relatively constant at a value $\sim 60\%$ greater than the original value. On the other hand, the zone appears to broaden even before crack growth starts. However, the width also attains a saturation value which is $\sim 60\%$ greater than after the initial cycle (Figure 4c).

The on-load and off-load strain profiles of the first fatigue cycle, including the COD and ϵ_c , appear to be identical within the experimental error (see Figure 5a). This result as well as the disparate behavior of the two ends of the crack are puzzling. While the crack tip strain profile on the right end assumed the steady state value prior to the fifth cycle (Figures 5b and 5d), the profiles on the left end appeared to be unaffected up to the onset of crack extension sometime between the 10th and 20th cycle. More experiments are needed to establish the significance of these results which may have been affected by heterogeneities in the foil, asymmetry of loading, and possibly, some tendency for the foil to buckle.

The results obtained after the onset of cracking appear to be more consistent. Figures 5b and d illustrate that a steady state was achieved quickly. Steady state values of the off-load COD and ϵ_c (which remained essentially unchanged throughout) were $\sim 60\%$ of the on-load values (see Figure 5c and Table 1). The on-load values were about 50% larger than those attending crack extension and stable crack growth during monotonic loading. Both the larger zones and the enhanced ductility may be connected with the cyclic softening⁽³³⁾ of the cold worked steel foil, an effect that has been observed on other materials. While these observations also lend support to the idea that fatigue crack growth proceeds with a constant of critical COD, they also suggest that this COD need not be the same as the value associated with the ordinary crack extension.

In the present experiments the material directly in front of the crack experienced about 200 cycles of reverse plastic strain.[†] Since the maximum strain range per cycle $= 2 \cdot [\epsilon_c(\text{on-load}) - \epsilon_c(\text{off-load})] = 0.25$ at the crack tip (see Table 1), the average plastic strain range over the entire zone length

[†] The number of plastic strain cycles $N = \rho \left(\frac{da}{dN} \right)^{-1}$, where ρ is the plastic zone length and $\frac{da}{dN}$ the crack advance per cycle. At steady state, $\rho = 0.040$ in., and $\frac{da}{dN} = 2.10^{-4}$ in.

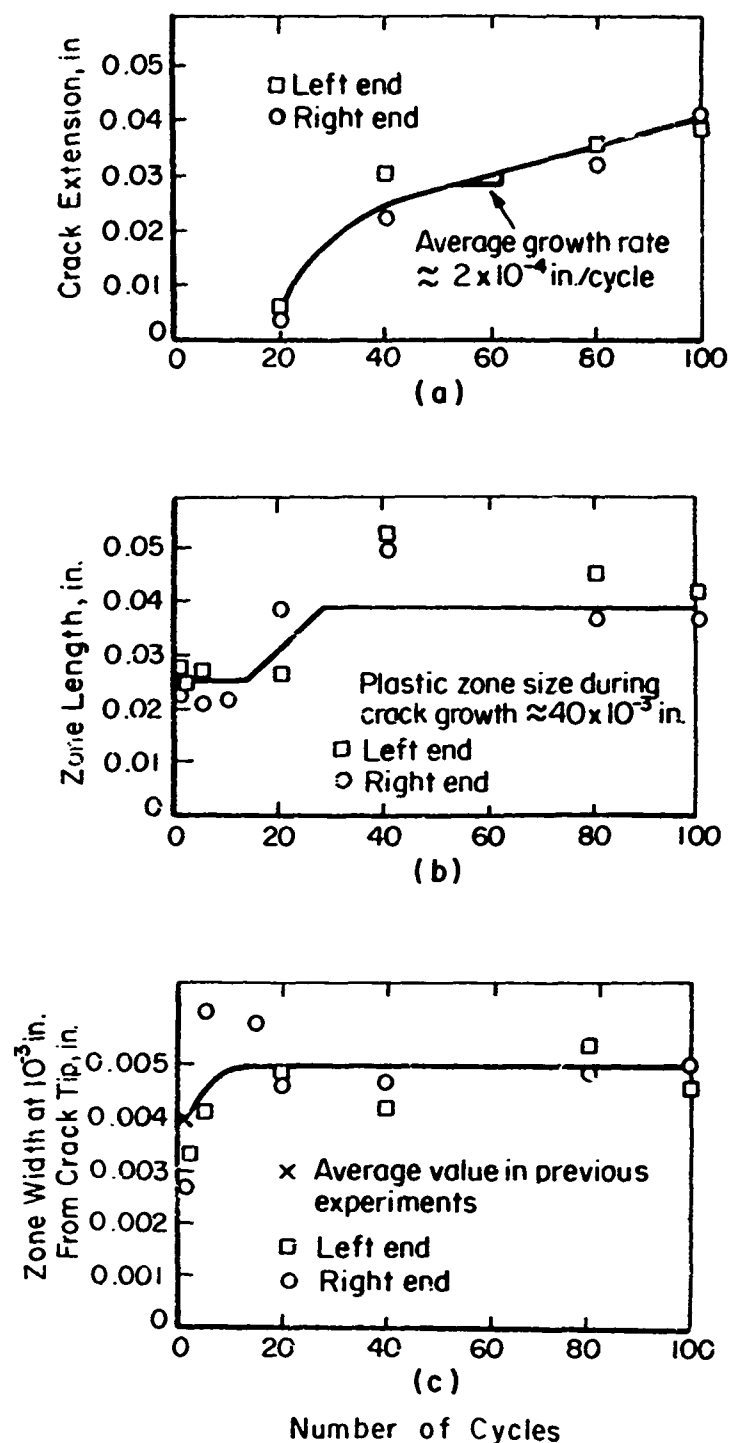


FIGURE 4. INFLUENCE OF CYCLIC LOADING, $\frac{\Delta K}{\sigma_y} = 0.225 \sqrt{\text{in.}}$, ON THE STEEL FOIL:
 (a) crack length, (b) plastic zone length, and (c) plastic zone width

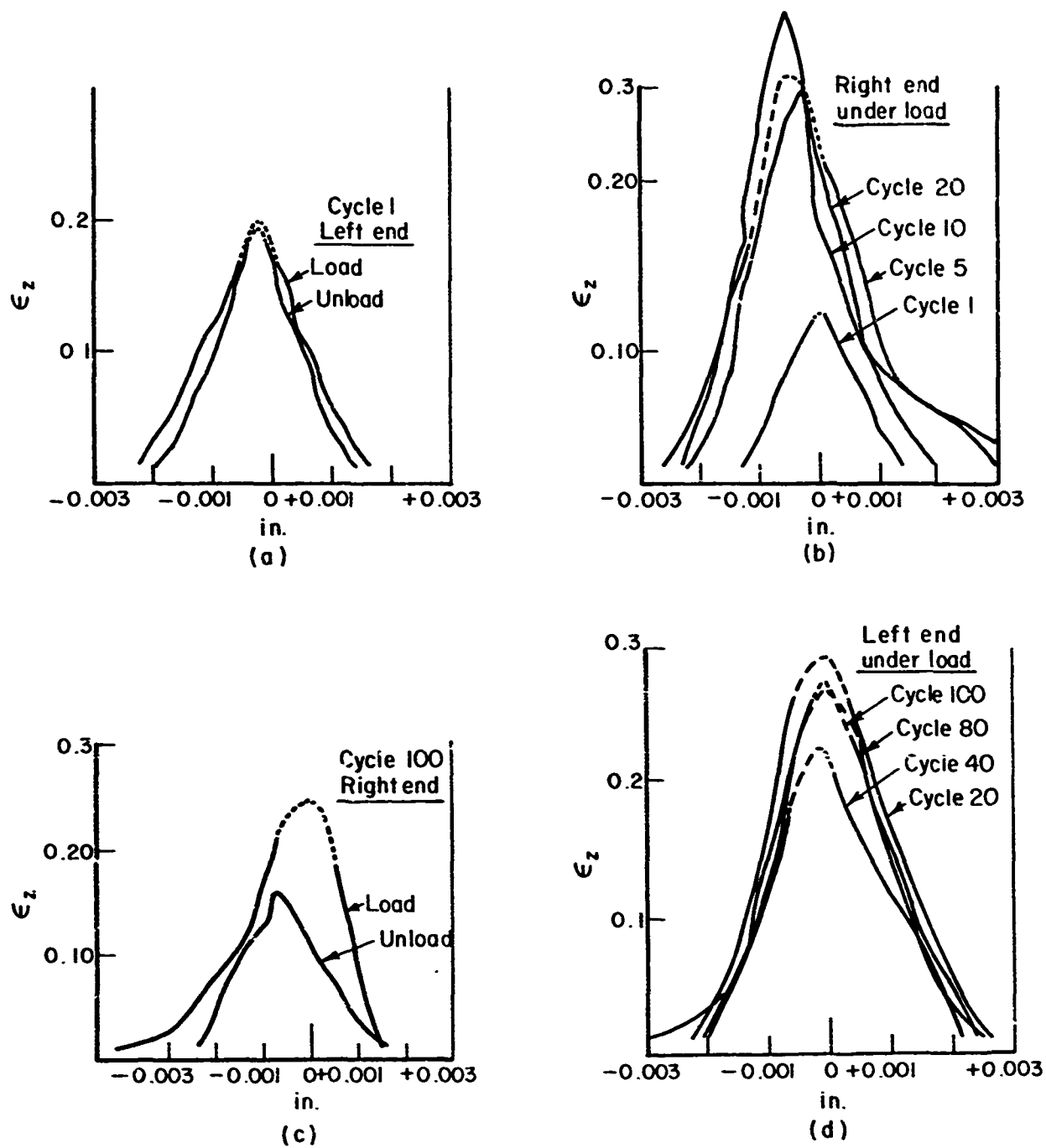


FIGURE 5. INFLUENCE OF CYCLIC LOADING ON THE CRACK TIP ϵ_z -STRAIN PROFILES: (a) and (d) for left end, (b) and (c) for right end

TABLE 1. SUMMARY OF COD AND CRACK-TIP STRAIN VALUES

| Type of Cracking | $\frac{K}{\sigma_Y}$ (in ^{1/2}) | COD | |
|--|---|-----------------------|--------------|
| | | (10 ⁻⁴ in) | ϵ_c |
| Stable crack growth under monotonic loading ⁽⁴⁰⁾ | 0.32-0.35 | 2.6 | 0.24 |
| Fatigue Crack Growth | | | |
| 1st Cycle, Load-on | 0.25 | 2.0 | 0.20 |
| 1st Cycle, Load-off | 0.025 | 1.7 | 0.17 |
| 20th-100th Cycle, Load-on | 0.25 | 3.9 | 0.31 |
| 20th-100th Cycle, Load-off | 0.025 | 2.3 | 0.185 |

is about 1/2 this value, or $\overline{\Delta\epsilon_p} \sim 0.1$, since the strain gradient is nearly linear⁽⁴⁰⁾. Thus, the total plastic strain accumulation prior to cracking, $\overline{\Delta\epsilon_p} \sim 20$ (85 times the value, 0.24, associated with failure under monotonic loading). Such strains could be accumulated if the material in front of the crack in the steel foil obeys a Manson-Coffin-type fatigue damage law⁽³⁵⁻³⁶⁾. Furthermore, a strain range $\overline{\Delta\epsilon_p} \sim 0.1$ is roughly consistent with expectations for a life of ~ 100 cycles based on unnotched tests on a large number of materials⁽⁴⁴⁾.

Plane Strain

The plastic zone produced in the DCB-specimen by the fatigue simulation procedure is shown in Figure 6. It can be compared with the zone of a stationary slit after one load-unload cycle reproduced in Figure 7 and with the zone of a slit cut-in under load at constant K without intermittent cycling in Figure 8. The size of the zone at the crack tip is essentially the same in all three cases (see Table 2)[†]. On the basis of the relation between zone size and COD shown to exist for simplified elastic plastic models^{††}, the COD's and near tip strain distributions should also be similar. This is in accord with the close-ups of the etched tip of the stationary slit and the one cut in at constant-K.^{†††} However, when the slit (or crack) is subjected to cyclic loading, the deformation from a number of zones will be superimposed at the crack tip (depending on the growth per cycle relative to the forward extent of the zone). The zone produced by cutting-in with intermittent unloading (Figure 6b) does, in fact, show a larger light etching zone at the crack tip^{†††} consistent with this picture.

The plastic zones and fracture morphologies of cracks produced by actual cyclic growth are shown in Figures 9-11. It is apparent from the pictures of the plate midsections, Figure 9, that the cyclic growth process was accompanied by some cleavage cracking. The fatigue portions of the failures are characterized by extensive light-etching regions on either side of the crack reflecting the superposition of deformations and resulting strain accumulation, and by the very ragged, irregular crack path with numerous instances of branching (see Figure 9c,d,g, and 10c). In some places the photos show irregularities on the crack path on a scale approaching the crack advance per cycle: $\sim 2 \cdot 10^{-5}$ in.

† For convenience, the quantity ρ , which is referred to as the zone size is defined here as the furthest extent of the etched region from the slit on the plate midsection measured normal to the plane of the slit.

†† $COD = \left(\frac{8}{\pi} \frac{\sigma_Y}{E} \right) \rho$, where ρ is the zone size, E is the elastic modulus and σ_Y is the yield stress⁽⁴³⁾. This relation is valid at relatively low nominal stress levels σ : $\sigma < 0.7 \sigma_Y$.

††† When the Fe-3Si Steel is strained more than $\sim 5\%$, it no longer etches dark. The interface between the dark and light etching region at the slit tip can be regarded as an isostrain contour corresponding to about 5%.



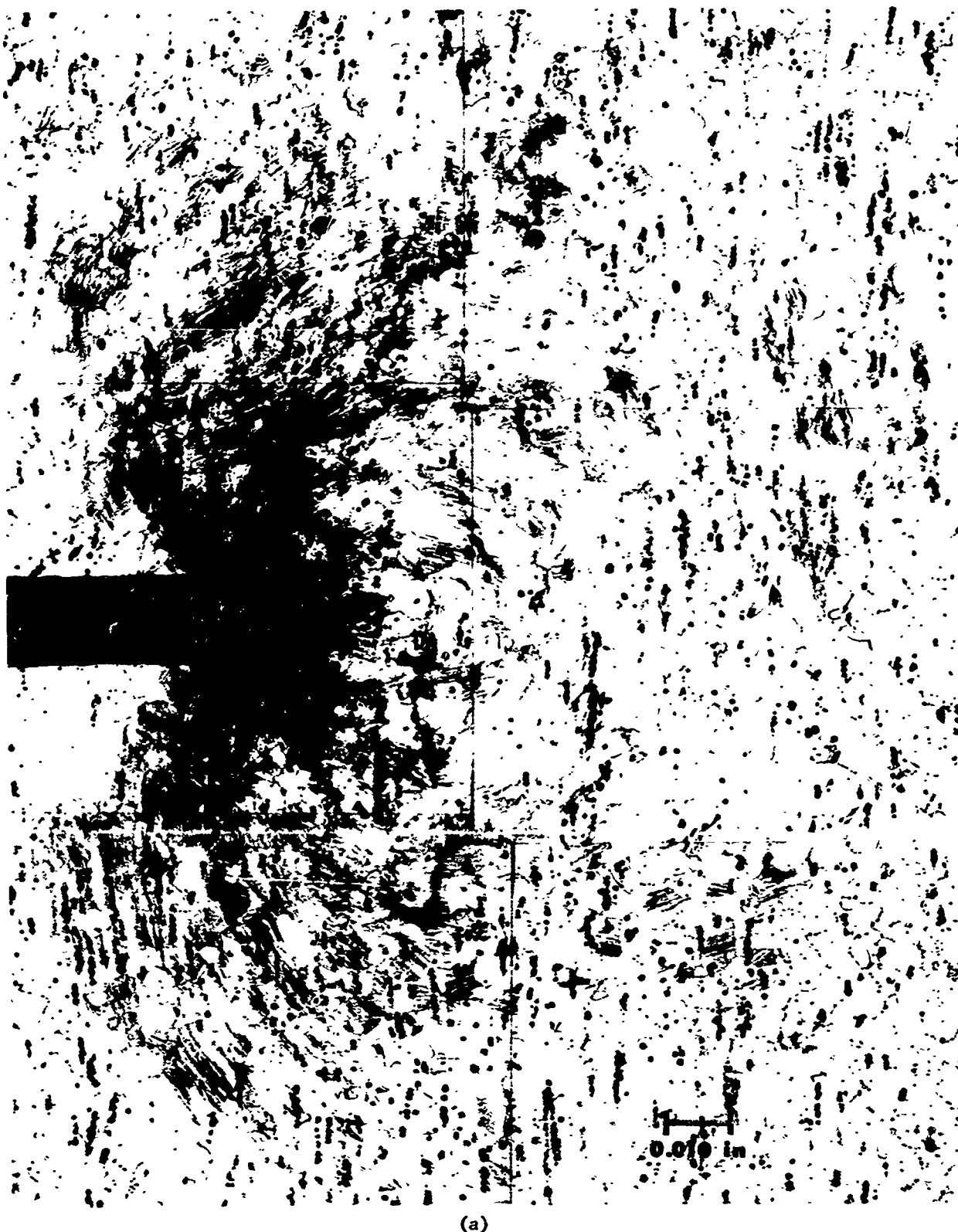
(a)

FIGURE 6. PLASTIC ZONE PRODUCED IN THE INTERIOR OF SPECIMEN 3P-20 BY THE FATIGUE SIMULATION PROCEDURE. The slit was cut in under loads corresponding to $\frac{K}{\sigma_Y} = 0.7 \sqrt{\text{in.}}$ in 50-0.0008 in. increments with intermediate unloading:

(a) zone revealed on specimen midsection, and (b) close-up of slit tip



(b)
FIGURE 6. PLASTIC ZONE PRODUCED BY FATIGUE SIMULATION PROCEDURE (Continued)



(a)

FIGURE 7. PLASTIC ZONE PRODUCED IN THE INTERIOR OF SPECIMEN 3P-19 BY MONOTONIC LOADING SIMULATION. Pre-cut, virgin slit was loaded once to $\frac{K}{\sigma_y} = 0.7 \sqrt{\text{in}}$ and unloaded: (a) zone revealed on specimen midsection, and (b) close-up of slit tip



(b)

FIGURE 7. PLASTIC ZONE PRODUCED IN THE INTERIOR OF SPECIMEN 3P-19 BY MONOTONIC LOADING SIMULATION (Continued)



(a)

FIGURE 8. PLASTIC ZONE PRODUCED IN THE INTERIOR OF SPECIMEN 3P-18 BY THE STABLE GROWTH SIMULATION PROCEDURE.⁽⁴³⁾ The slit was cut in under loads corresponding to a constant stress intensity, $\frac{K}{c\sqrt{y}} = 0.7 \sqrt{\text{in}}$: (a) zone revealed on specimen midsection and (b) close-up of slit tip



(b)

FIGURE 8. PLASTIC ZONE PRODUCED IN THE INTERIOR OF SPECIMEN 3P-18 BY THE STABLE GROWTH SIMULATION PRO-
CEDURE (43) (Continued)

TABLE 2. SUMMARY OF PLASTIC ZONE SIZE-VALUES OBTAINED FROM ETCHING EXPERIMENTS

| Spec. No. | Description of Experiment | $\frac{K_{\infty}}{\sigma_Y}$ (in ^{1/2}) | Cyclic Growth Rate (in) | Zone Size, ρ (in) | |
|-----------|---|--|-------------------------|------------------------|------------------|
| | | | | Plate Surface | Plate Midsection |
| 3P-19 | Pre-cut slit subjected to one load-unload cycle | 0.7 | - | 0.058 | 0.075 |
| 3P-23 | " | 0.7 | - | 0.053 | 0.069 |
| 3P-18 | Slit cut in under load at constant stress intensity | 0.7 | - | 0.055 | 0.074 |
| 3P-20 | Slit cut in under load with intermediate load cycling | 0.7 | $8 \cdot 10^{-4}$ | 0.058 | 0.070 |
| 3P-24 | Fatigue Crack Growth | 0.7 | $\sim 2 \cdot 10^{-5}$ | 0.065 | 0.070 |
| 3P-25 | " | 0.7 | $1.2 \cdot 10^{-5}$ | 0.046 | 0.060 |



(a) Plastic zone revealed on specimen surface

FIGURE 9. PLASTIC ZONE OF A MIXED FATIGUE-CLEAVAGE CRACK PRODUCED IN SPECIMEN 3P-24 BY 21,770 CYCLES WITH A STRESS INTENSITY RANGE $\frac{\Delta K}{\sigma_y} = 0.7 \sqrt{\text{in}}$ (CLEAVAGE PORTIONS ARE LABELED C)



(b) Continuation of zone on specimen surface

FIGURE 9. PLASTIC ZONE OF A MIXED FATIGUE-CLEAVAGE CRACK IN SPECIMEN 3P-24 (Continued)

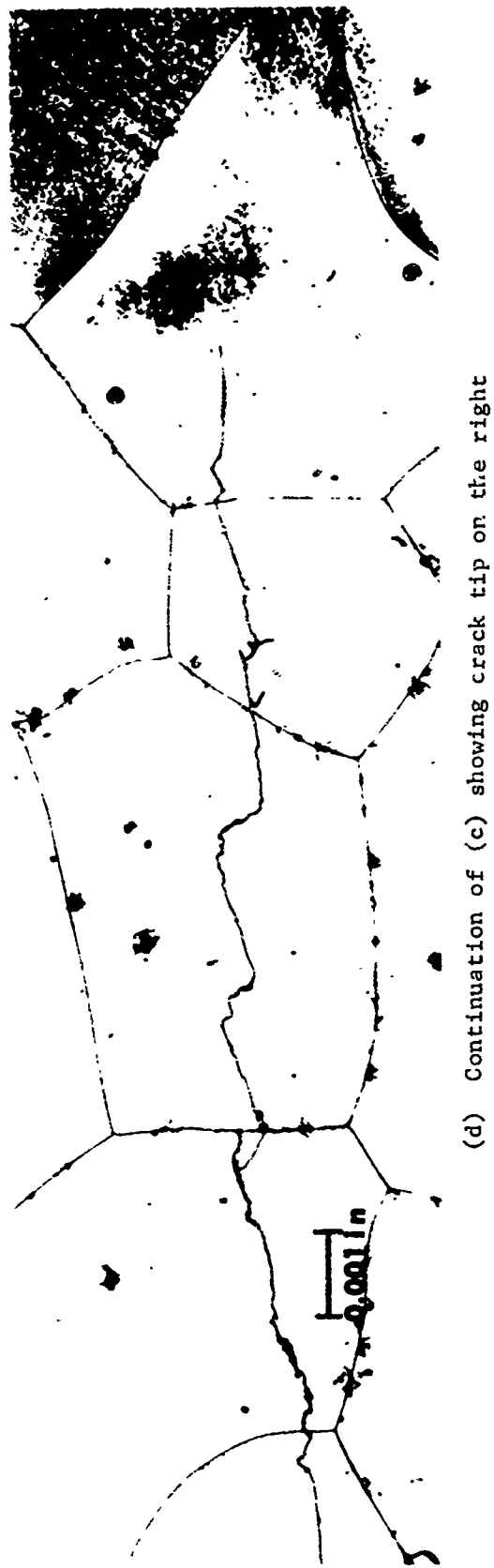
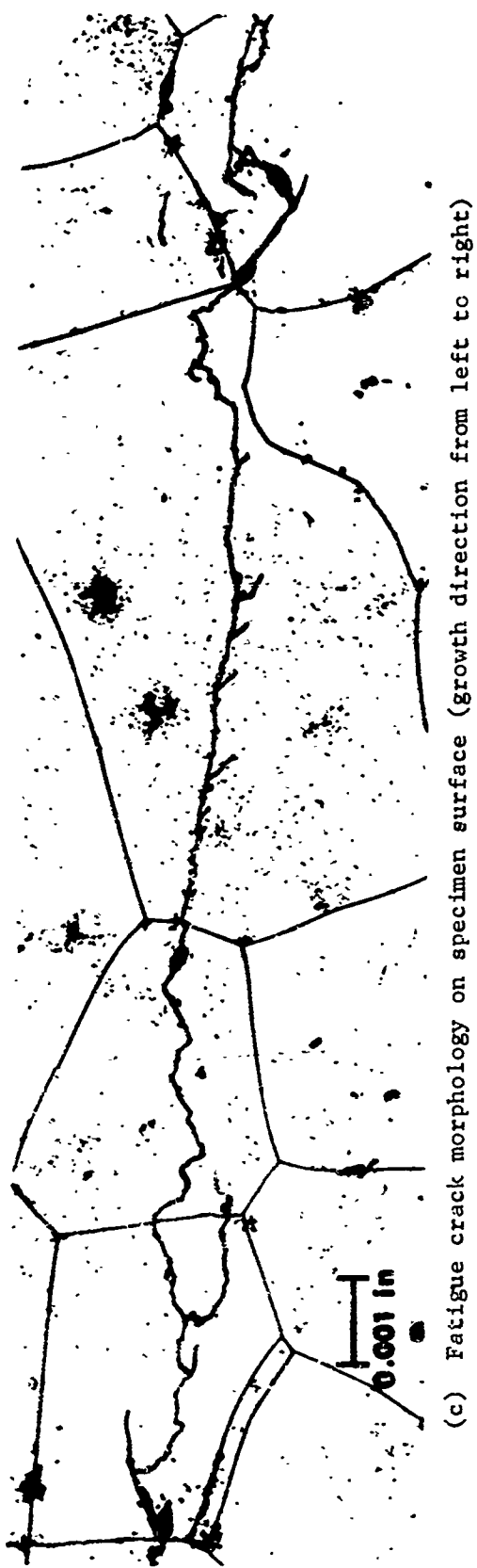


FIGURE 9. PLASTIC ZONE OF A MIXED FATIGUE-CLEAVAGE CRACK IN SPECIMEN 3P-24 (Continued)



(e) Plastic zone revealed in the interior on specimen midsection

FIGURE 9. PLASTIC ZONE OF A MIXED FATIGUE-CLEAVAGE CRACK IN SPECIMEN 3P-24 (Continued)



(f) Continuation of zone revealed in the interior on specimen midsection

FIGURE 9. PLASTIC ZONE OF A MIXED FATIGUE-CLEAVAGE CRACK IN SPECIMEN 3P-24 (Continued)



(a) Plastic zone revealed on specimen surface

FIGURE 10. PLASTIC ZONE OF A MIXED FATIGUE-CLEAVAGE CRACK PRODUCED IN SPECIMEN 3P-25 BY 9930 CYCLES WITH A STRESS INTENSITY RANGE $\frac{\Delta K}{\text{Cy}} = 0.7 \sqrt{\text{in}}$ (CLEAVAGE PORTIONS ARE LABELED C)



(b) Plastic zone revealed in the interior on the specimen midsection

FIGURE 10. PLASTIC ZONE OF A MIXED FATIGUE-CLEAVAGE CRACK IN SPECIMEN 3P-25 (Continued)



(c) Morphology of the fatigue crack on the specimen midsection

FIGURE 10. PLASTIC ZONE OF A MIXED FATIGUE CLEAVAGE CRACK IN SPECIMEN 3P-25 (Continued)



(d) Morphology of mixed cleavage and fatigue portions of the crack on the specimen midsection

FIGURE 10. PLASTIC ZONE OF A MIXED FATIGUE-CLEAVAGE CRACK IN SPECIMEN 3F-25 (Continued)

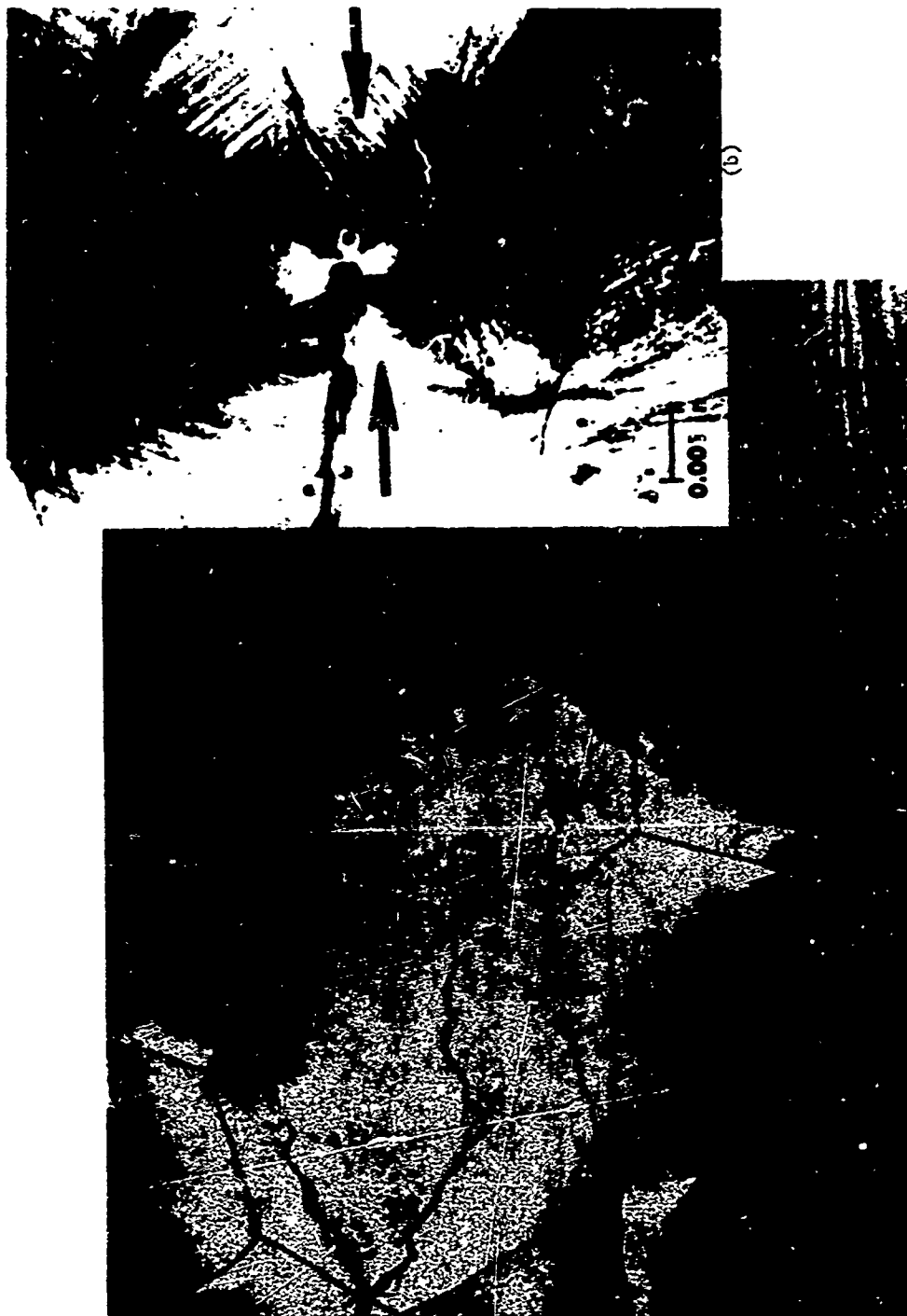


FIGURE 11. COMPARISON OF FATIGUE CRACK- AND STATIONARY, VIRGIN CRACK-NEAR-TIP PLASTIC ZONES: (a) tip of fatigue crack of Specimen 3P-25 growing at $\sim 10^{-5}$ in. per cycle at $\Delta K \sim 0.5 \sqrt{\text{in.}}$, and (b) virgin crack loaded to $\frac{\Delta K}{\sigma_y} = 0.4 \sqrt{\text{in}}$ and unloaded (4).

NOTE: The J light etching region near the crack tip is the region strained plastically in excess of 5%. This region has essentially the same shape in both cases including the small protuberance directly in front of the crack. Taking into account the difference in stress intensity levels, the 5%-strain-region surrounding the fatigue crack is still substantially larger as a result of the accumulation of plastic strain during reverse cycling.

The crack branches seem to have an included angle $\sim 90^\circ$ and are in all cases at least 10 x larger than the average crack growth per cycle, a sign that the branches represent not merely nucleation but many cycles of growth. The branches suggest there are two alternate and symmetric sites near the tip of the main fatigue crack for the cyclic growth, and that the two sites occasionally operate simultaneously. Similar observations have been reported and are discussed by Laird⁽³³⁾. It is also interesting to note that some of the branches were arrested at grain boundaries (see Figure 9g).

Table 2 illustrates that the fatigue crack plastic zone size is essentially the same as that displayed by the slits that were loaded to the same peak stress intensity level. Previous experience shows that the size of the zone attending a sharp crack is essentially the same as the slit zone-size (when the extent of the zone is much larger than the slit-tip radius). Thus, the result derived from actual fatigue cracks and simulation experiment are the same: namely, there does not seem to be a significant difference in the plastic zone size of a cyclically loaded, growing crack and the monotonically loaded crack under plane strain conditions.

Figure 11 compares the near-tip strain distributions of a fatigue zone with a monotonic zone⁽⁴¹⁾ at comparable stress levels[†]. It can be seen that the light etching regions of both the monotonic zone display small protuberances directly in front of the crack. It seems likely that these are manifestations of the intensely strained region near the tip of the crack (see Figure 12a) recently treated by Rice and Johnson⁽²⁹⁾. The shape of light etching region near the tip can be rationalized in terms of the slip line field and the superposition of the two symmetric enclaves directly in front of the crack as shown in Figure 12b. The existence of protuberances in both zones is further evidence that the basic character of the strain distribution is not altered by cycling. The fatigue zone does display a larger light etching region and this is consistent with the superposition and accumulation of deformation from successive cycles.

DISCUSSION

The main finding here is there are no striking differences between fatigue crack zones--those produced in the foil and in the Fe-3Si plate by simulation and actual cracking--and the corresponding monotonic zones. While no radical differences were anticipated, the result is at odds with the expectation, discussed by Rice⁽²⁸⁾ that the steady-state cyclic zone is 1/4 the size of the stationary monotonic zone^{††}. The discrepancy may simply be a consequence of the yield stress reduction affected by cycling (Bauschinger effect in the

† The stress intensity level associated with the fatigue crack tip on the specimen midsection is less than the applied stress intensity level $\left(\frac{\Delta K}{\sigma_Y} \approx 0.7 \sqrt{in}\right)$ because the crack tunneled. The value quoted in Figure 12: $\frac{\Delta K}{\sigma_Y} \sim 0.05 \sqrt{in}$ is an estimate based on the actual size of zone, and $\frac{\Delta K}{\sigma_Y}$ - zone size relation developed for this DCB-specimen configuration⁽⁴⁵⁾.

†† For cycling between zero stress intensity and a peak value.

Fe-3Si steel and cyclic softening in the cold worked foil). Cyclic stress-strain measurements for these materials are needed to establish whether the reductions are large enough to account for the zones.

While questions remain, the observed similarities in size, shape and strain distribution do support the practice of applying the monotonic functional relations to the cyclic growth problem. For example, previous calculations and etching experiments indicate that the dimensions ρ , l , l' , and COD under plane strain (see Figure 12a) can be approximated by the following expressions (28,29,41,46):

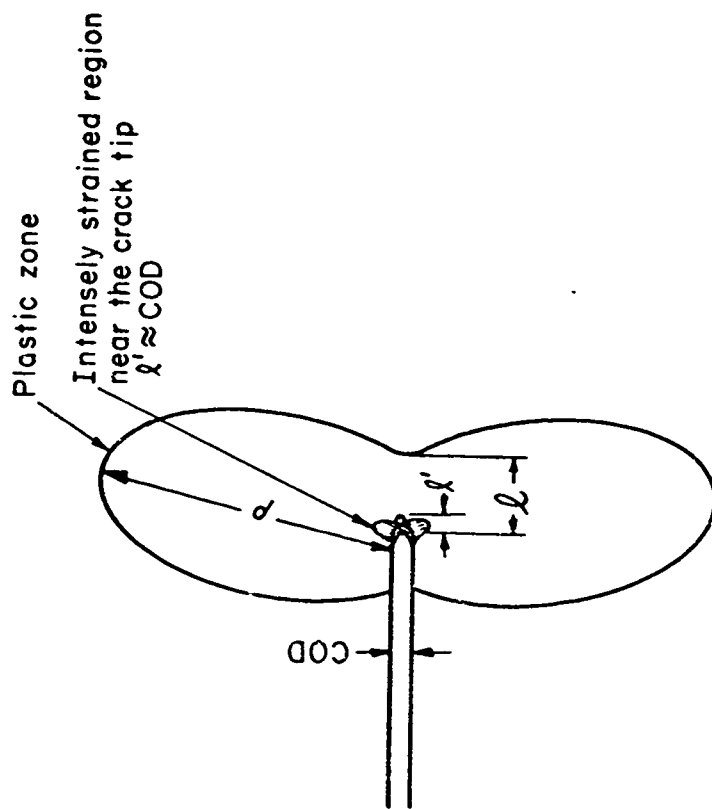
| MONOTONIC ZONE | CYCLIC ZONE |
|--|---|
| $\rho \approx 0.2 \left(\frac{K}{Y} \right)^2 \dots (1A)$ | $\rho \sim 0.2 \left(\frac{\Delta K}{2Y_c} \right)^2 \dots (1B)$ |
| $l \approx 0.03 \left(\frac{K}{Y} \right)^2 \dots (2A)$ | $l \sim 0.03 \left(\frac{\Delta K}{2Y_c} \right)^2 \dots (2B)$ |
| $l' \approx \text{COD}$ | $l' \sim \text{COD} \dots (3)$ |
| $\text{COD} \approx \frac{K^2}{2EY} \dots (4A)$ | $\text{COD} \sim \frac{\Delta K^2}{4EY_c} \dots (4B)$ |

where K is the stress intensity, Y is the uniaxial yield stress, E the elastic modulus, ΔK the stress intensity range, Y_c the cyclic yield stress and COD the crack opening displacement. The observation that $\rho(\text{monotonic}) \approx \rho(\text{cyclic})$ for the Fe-3Si Steel (see Table 2) suggests that $Y \approx 2Y_c$. As will be discussed later, this is only likely to be true in the lightly strained region that controls the outward reach of the plastic enclave, and not in the heavily deformed region that affects the value of l' and COD. The number of cycles of plastic straining experienced by material in front of the crack is:

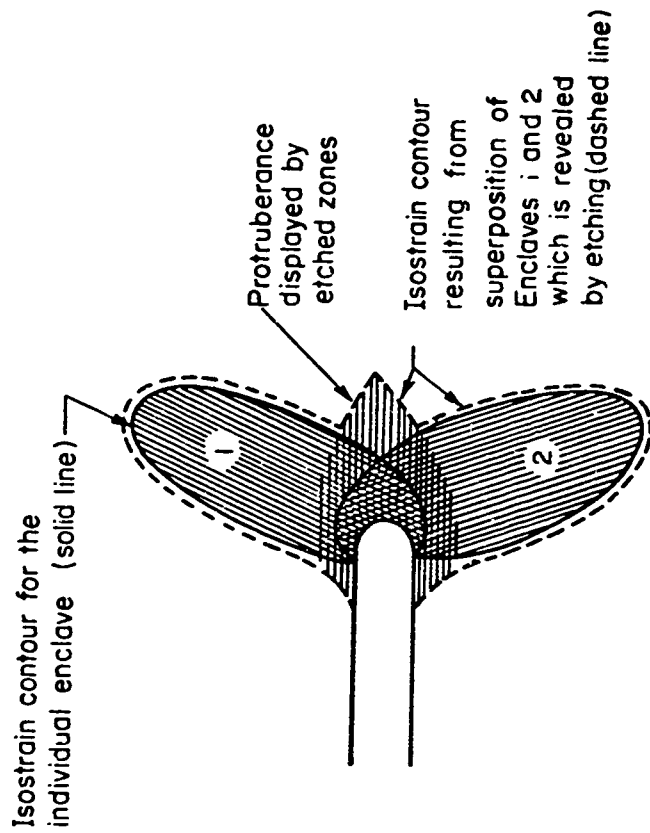
$$\eta = \frac{l}{\frac{da}{dN}} \sim \frac{0.03\Delta K^2}{\frac{da}{dN} 4Y_c^2} \sim \frac{0.03\Delta K^2}{\frac{da}{dN} Y^2} \quad (5)$$

$$\eta' \approx \frac{l'}{\frac{da}{dN}} \sim \frac{\Delta K^2}{\frac{da}{dN} 4EY_c} \quad (6)$$

where η is the total number of cycles of plastic strain, and η' the number of cycles of large plastic strains located within the intensely strained near tip region. (29) Estimates obtained in this way, assuming either $Y_c = Y$ and $Y_c = 2Y$, are listed in Table 3 for 3 different materials. The relative invariance of the calculated values of η and η' is an indication that crack growth rates are scaled to the dimensions of the plastic zone. A crude estimate of the total



a.



b.

FIGURE 12. SCHEMATIC OF MONOTONICALLY LOADED CRACK TIP PLASTIC ZONE: (a) plastic enclave identifying dimensions, (b) slip line field pattern and (c) near tip, high strain contours

TABLE 3. ESTIMATES OF N AND N' , THE NUMBERS OF PLASTIC STRAIN CYCLES AND β , THE RATIO OF CRACK GROWTH PER CYCLE TO CRACK-OPENING DISPLACEMENT

| Material | \bar{Y} (ksi) | Reference | $\frac{da}{dN}$ in/cycle | ΔK ksi $\sqrt{\text{in}}$ | $N_c = Y$ N | β | $N_c = 2Y$ N | N' | β |
|---------------|--------------------|---------------------|-----------------------------|--------------------------------------|-------------------|-------------------|-------------------|------|---------|
| 7075-T6 | ~ 72 | Liu and Iino (22) | 10 ⁻³ | 37 | 10 ^(a) | ~1 ^(a) | 5 ^(a) | ~1 | >1 |
| | | | 10 ⁻⁴ | 24 | 30 | 2 | 15 | ~1 | ~1 |
| | | | 10 ⁻⁵ | 11 | 70 | 4 | 35 | 2 | 0.5 |
| | | | 10 ⁻⁶ | 4.6 | 120 | 7 | 60 | 4 | 0.3 |
| | | | | | | | | | |
| HY-130 | ~140 | Barsom, et al. (24) | 10 ⁻³ | 140 | 30 ^(a) | ~1 ^(a) | 15 ^(a) | ~1 | >1 |
| | | | 10 ⁻⁴ | 83 | 110 | 4 | 55 | 2 | 0.5 |
| | | | 10 ⁻⁵ | 29 | 130 | 5 | 65 | 3 | 0.4 |
| | | | 10 ⁻⁶ | 10 | 150 | 6 | 75 | 3 | 0.3 |
| | | | | | | | | | |
| 10Ni-Cr-Mo-Co | ~190 | Barsom, et al. (24) | 10 ⁻³ | 165 | 20 ^(a) | ~1 ^(a) | 10 ^(a) | ~1 | >1 |
| | | | 10 ⁻⁴ | 85 | 60 | 3 | 30 | 2 | 0.7 |
| | | | 10 ⁻⁵ | 35 | 100 | 5 | 50 | 3 | 0.4 |
| | | | 10 ⁻⁶ | 13 | 140 | 7 | 70 | 4 | 0.3 |
| | | | 10 ⁻⁷ | 5 | 200 | 11 | 100 | 5 | 0.2 |

(a) Probably an underestimate because plane strain conditions not satisfied.

accumulated plastic strain can also be derived: $2\Delta\epsilon_p \eta' \sim 7^\dagger$. This suggests that the flow stress for deformation near the crack tip could be raised substantially by strain hardening, and for this reason, estimates are also given in Table 3 for $Y_c = 2Y$.

Equations 1-4 are used in Appendix B to derive simplified expressions of the growth rates implied by the two mechanisms of crack advance that have currency:

- (1) Irreversible Plastic Blunting (Kinematic Irreversibility) (32-34). The crack advances because the deformation attending the unloading part of the cycle is not an exact reversal of the deformation that blunts the crack during loading:

$$\frac{da}{dN} \sim \beta \frac{\Delta K}{4EY_c} \quad (7)$$

$$\text{and } \left\{ \begin{array}{l} \frac{da}{dN} \sim 4 \left(\frac{\Delta K}{E} \right)^2 \\ \text{for } Y_c = 0.01E, \beta = 0.15 \end{array} \right. \quad (7A)$$

- (2) Damage Accumulation (22,31). The actual rupture of regions damaged by the succession of plastic strain cycles experienced by material in front of the crack:

DAMAGE ACCUMULATION

Large Strains:

$$\frac{da}{dN} \sim \frac{\Delta\epsilon_p^2}{4B^2EY_c} \Delta K^2 \quad (8)$$

$$\left\{ \begin{array}{l} \frac{da}{dN} \sim 25 \left(\frac{\Delta K}{E} \right)^2 \\ \text{for } \frac{\Delta\epsilon_p^2}{B^2} = 1, Y_c = 0.01E \end{array} \right. \quad (8A)$$

Small Strains:

$$\frac{da}{dN} \sim \frac{0.1}{B^2} \left(\frac{\Delta K}{E} \right)^2 \quad (9)$$

$$\left\{ \begin{array}{l} \frac{da}{dN} \sim 0.2 \left(\frac{\Delta K}{E} \right)^2 \\ \text{for } B^2 = 0.5 \end{array} \right. \quad (9A)$$

$\dagger \eta' \sim 5$ for $\frac{da}{dN} = 10^{-5}$ and $Y = Y_c$, and $\Delta\epsilon_p$, the weighted average strain range close to the crack tip corresponds to the average strain in the monotonically loaded zone at distances smaller than the COD and is ~ 0.7 (29).

The quantity $\beta \equiv \frac{da}{dN}/COD$ is the efficiency of the blunting process, B is a measure of ductility, and $\Delta\bar{\epsilon}_p$, the weighted average plastic strain range per cycle. These expressions are similar to the empirical growth rate law obeyed by a wide range of alloys in Regime No. 1 (see Appendix A and Tables 4 and A-i):

$$\frac{da}{dN} \approx A' \left(\frac{\Delta K}{E} \right)^2 \quad (10)$$

where $A' \sim 8$. The experiments thus provide a way of examining the two mechanisms critically:

- a. Stress Intensity Dependence. Both mechanisms can account for the experimentally observed stress intensity exponent: $m \approx 2$, which applies to both the microscopic growth rate and the striation spacing in Regime No. 1. (See results of Broek⁽²¹⁾ on 7075-T6 and Miller⁽²⁶⁾ on 4340 and 18 Ni-Maraging Steel in Table A-1.
- b. Absence of a Yield Strength Dependence. Tables 4 and A-1 illustrate that crack growth rates in Regime No. 1 are independent of the yield stress level for a wide range of materials. At first glance this result appears to favor the "small strain" damage accumulation argument since the other two treatments predict a dependence on Y_c (Equations 7 and 8). However, Y_c is not the ordinary yield stress but the cyclic yield or flow stress. Evidence is presented in Appendix C that the COD is most strongly influenced by the value of flow stress appropriate for the heavily strained material close to the crack tip. Since the rate of strain hardening varies inversely with strength level, it is possible that the cyclic flow stress at high strains approaches a common level, e.g., $Y_c \sim \frac{E}{100}$, for all materials. By way of this argument, which was suggested by Laird⁽⁴⁷⁾, the absence of a yield stress dependence can be rationalized with either mechanism (see Equations 7A and 8A).
- c. Modulus Dependence. Table 4 illustrates that when the resistance cyclic crack growth is normalized with respect to modulus in Regime 1, the $\frac{\Delta K}{E} \big|_{10^{-5}}$ values are nearly the same irrespective of alloy system. This feature, noted earlier by Bates and Clark⁽¹⁵⁾, is consistent with both mechanisms provided Y_c is a fixed fraction of E (see Equations 7A and 8A).
- d. Absence of a Ductility Effect. Table 4 shows that steels known to possess different levels of ductility still display the same resistance to crack growth. This seems to be inconsistent with the damage accumulation mechanism. However, it can also be argued here that the ductility in question is not the ordinary smooth bar value, but the value for a highly localized region under a complex state of stress, and this could be relatively invariant.

TABLE 4. SUMMARY OF SELECTED CYCLIC CRACK GROWTH RESISTANCE VALUES (See Table A-1 for Entire Compilation)

| Material | σ (Ksi) | $\Delta K \left \frac{da}{dN} = 10^{-5} \text{ in} \right $ (Ksi $\sqrt{\text{in}}$) | $\Delta K \left \frac{da}{dN} = 10^{-5} \text{ in} \right $ $10^{-3} \sqrt{\text{in}}$ | ΔK_{1-2} (Ksi $\sqrt{\text{in}}$) | Reference |
|------------------------|-------------------|---|--|---|--|
| Fe-3Si | 54 | ~ 38 | 1.3 | - | Present Study (15) |
| 3Ni-Mo-V | 93 | 39 | 1.3 | - | Bates and Clark (24) |
| HY-80 | 95 | 33 | 1.1 | - | Barson, et al. (18,26) |
| HY-130 | 140 | 29.5 | 1.0 | 92 | " |
| 4340(Q & T at 1000° F) | 163 | 33 | 1.1 | 80 | Miller (18,26) |
| 10Ni-Cr-Mo-Co | 191 | 35 | 1.2 | 86 | Parson, et al. (23) |
| 18Ni-Maraging | 218 | 31 | 1.0 | 80 | Miller (18,26) |
| 18Ni-Maraging | 246/252 | 36 | 1.2 | 80 | Wei, et al. (12) and Carman and Katlin (8) |
| H11 | 242 | 34 | 1.1 | - | Carman and Katlin (8) |
| D6AC | 241 | 32 | 1.1 | ~ 70 | " |
| 5456-H321 | 37 | 12 | 1.2 | - | Bates and Clark (15) |
| 2024-T3 | 50 | 9.5/13 | 1.0/1.3 | 29 | Forman, et al. (9), Donaldson and Anderson (4), McEvily and Illg (2), Hudson and Hardvath (5), Weibull (1) |
| 2024-T3 | 50 | 10.5 | 1.1 | 16 | Broek and Schijve (6) |
| 7075-T6 | 70 | 14 | 1.4 | - | Broek (21) |
| 7075-T6 (Argon) | 70 | 10 | 1.0 | 20 | " |
| 7075-T6 | 70 | 14.5 | 1.5 | - | Wei and Landes (27) |
| 7079-T6 | 65 | 7.5 | 0.8 | 22 | " |
| | | 12 | 1.2 | - | Bates and Clark (15) |
| Ti-6Al-4V | 127 | 15 | 0.9 | - | " |
| 70-30 Brass | 18 | 14 | 0.9 | - | McEvily, et al. (7) |
| 70-30 Brass | 92 | 14 | 0.9 | - | " |

- e. Efficiency of the Blunting and Damage Accumulation Mechanisms. Relatively little is known about the efficiency (degree of irreversibility) of the blunting process. A value of $\beta \approx 0.15$ can be deduced directly in one case--from photographs of a relatively short, highly strained crack in a polyethylene sheet published by McEvily and co-workers⁽⁴⁹⁾--which define both the COD and $\frac{da}{dN}$. This value is reasonably close to the β -values calculated for three alloys in Table 3 for $Y_c = Y$. The higher value, $Y = 2Y$, associated with the heavily strained hardened region, implies a greater efficiency, e.g., $\beta = 0.3-0.4$. Such an efficiency may well be unrealistic, but this is not significant since the calculations of COD could well be in error by a factor of 2. Viewed in this light there is reasonably good agreement between the absolute prediction of the blunting mechanism and experiment (between Equations 7A and 10). By the same token, the predictions derived from the "large strain" damage accumulation treatment, Equation 8A, are also reasonable, although the values of $\Delta\bar{\epsilon}_p$ and B are at present very poorly defined. While the "small strain" damage accumulation treatment is least satisfactory for plane strain, it is roughly in accord with the results for the steel foil as pointed out in a preceding section.
- f. Transient Crack Growth Rates. The damage accumulation mechanism implies that the material in front of a crack is conditioned by a number of plastic strain cycles. Consequently, the crack advance per cycle at a given ΔK should increase gradually and only approach the steady state value after some number of stress cycles. Similar transients should be observed whenever ΔK is increased abruptly; a gradually decreasing rate when ΔK is abruptly reduced. This expectation is not confirmed by photographs of the striations produced by programmed loads that have been published by McMillan and Pelloux⁽⁵⁰⁾ and Christensen and Harmon⁽⁵¹⁾ which show no signs of transients. This probably is the strongest argument against the damage accumulation mechanism. To the extent that strain accumulation from successive cycles contributes to the value of Y_c , transients having the opposite character should be associated with the blunting mechanism. While the striations mentioned above provide no clear-cut evidence of such transients either, the experiments of Hardrath⁽⁵²⁾ do show that a high pre-stress can retard the crack growth rate, and this is consistent with the expectation for blunting.
- g. Environmental Effects. The results of Barsom⁽²³⁾ on 12Ni-5Cr-3Mo and Wei and Landes⁽²⁷⁾ on 7075-T651 in Table A-1 show that certain "aggressive" environments greatly enhance the crack growth rate in Regime No. 1. This effect is difficult to understand in terms of the environments' effect on the flow stress and blunting and easier to rationalize in terms of rupture, and thus, damage accumulation.

Regime No. 1. The preceding paragraphs show that the main features of the low stress-high cycle portion of the growth rate spectrum can be explained either in terms of the plastic blunting or the damage accumulation mechanism.

While neither mechanism is entirely satisfactory, irreversible blunting seems to be consistent with more observations at the present time.

Regime No. 2. The mechanism of growth in Regime No. 2, the high stress-low cycle range is not well defined. A possible clue is the observation that macroscopic (or average) crack advance per cycle exceeds the striation spacing^(15,21,26). This can begin to occur when brittle particles or other weak interfaces well in advance of the main crack front come under the influence of the plastic zone and rupture. These ruptures not only contribute to the crack advance per cycle, but may be sources of secondary fatigue cracks as suggested by the work of Erhardt and Grant⁽⁵³⁾. Thus the same mechanism operating in Regime No. 1 when augmented by an increasing length of active crack front (making A a stress dependent term) can account for (1) higher growth rates, (2) a greater stress dependence and (3) the discrepancy between growth rate and striation spacing (see Figure 13). Accordingly, ΔK_{1-2} : the stress intensity range at the transition from Regime No. 1 to Regime No. 2 should depend on the spacing and properties of specific microstructural features which may vary from alloy to alloy and heat to heat. Consistent with this, the ΔK_{1-2} -values listed in Tables 4 and A-1 are not constant and do not seem to correlate with yield strength. At higher stress intensity levels, the approach to general yielding and transition from plane strain to plane stress may also accelerate the crack growth rate.

This admittedly tentative picture could have important implications with respect to the metallurgical factors and alloy development. To the extent that environmental effects are not involved, neither Equation 10 nor the compilation of $\Delta K'$ values shows any systematic effects of composition, microstructure, or the usual thermal-mechanical treatments. It is true that metallurgical contributions amounting to $\sim \pm 20\%$ of ΔK_{10-5} (corresponding with $\sim 50\%$ change in total life) could be obscured by the scatter of the data. Beyond this, the prospects of improving crack growth resistance in Regime No. 1 by the usual techniques do not seem bright. It is possible that large improvements could be realized by metallurgical changes that are designed to eliminate susceptibility to aggressive environments. Special microstructures, such as composites with interfaces normal to the crack front that delaminate preferentially, may offer advantages. The micrographs in this report contain some evidence that fatigue cracks are impeded by grain boundaries, but it is not clear whether enough boundaries can be introduced to affect the average crack growth increment significantly⁽⁵⁴⁾.

In contrast, the behavior in Regime No. 2, especially the value of ΔK_{1-2} , could be quite sensitive to the microstructure, to the strength and spacing of hard particles and to other metallurgical factors if the explanation offered here is correct. Furthermore, significant improvements in total life can be achieved simply by increasing ΔK_{1-2} and postponing the higher growth rates generated in Regime No. 2. To test this possibility, it would be useful to compare ΔK_{1-2} -values obtained for a single phase alloy with modifications involving different distributions and morphologies of hard particles.

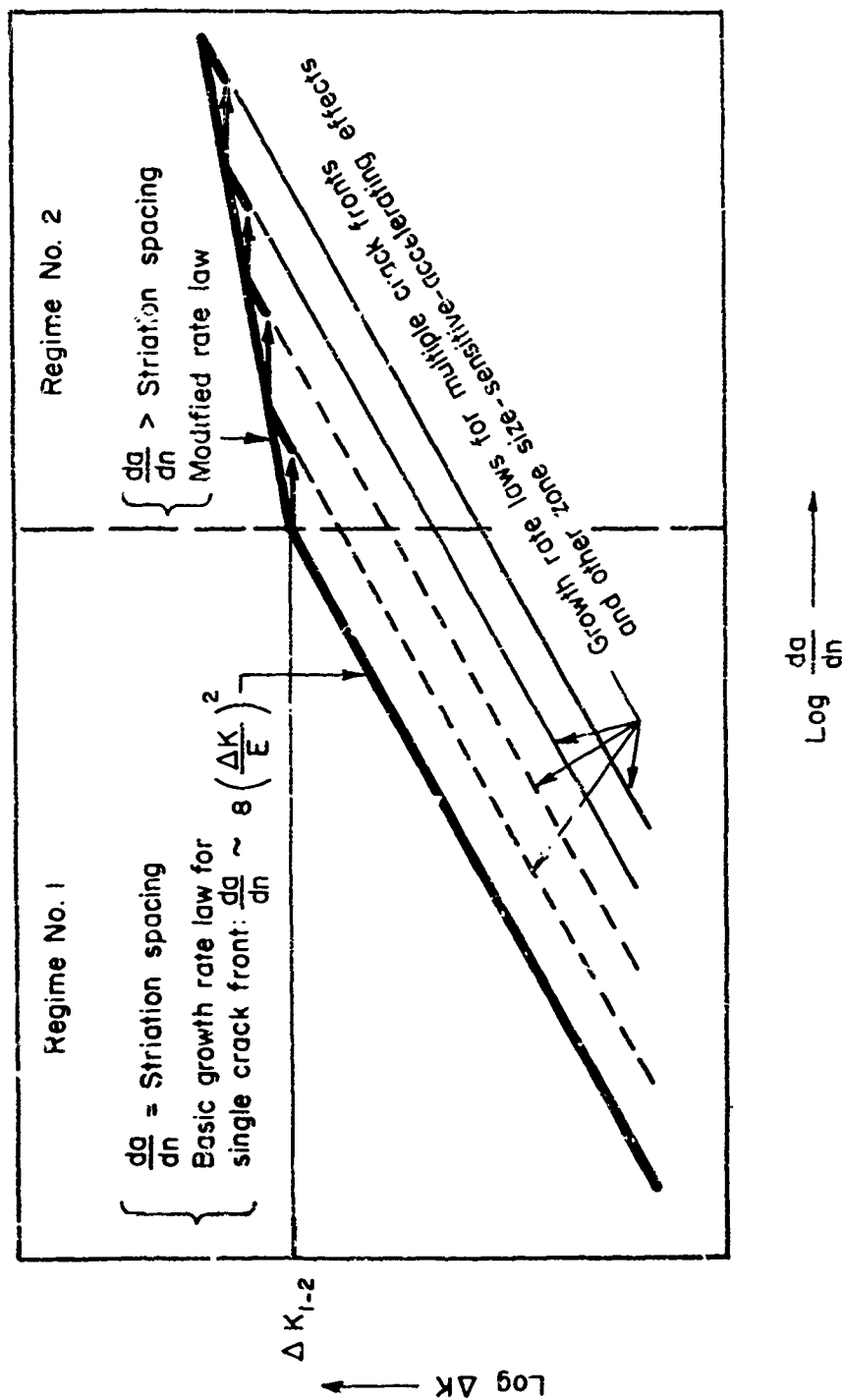


FIGURE 13. SIMPLIFIED SCHEMATIC REPRESENTATION OF THE ORIGIN OF REGIMES NO. 1 AND NO. 2

CONCLUSIONS

1. The interferometric technique applied to the steel foil and the etching technique for Fe-3Si can provide useful insights to the size of the fatigue crack plastic zone and the strain distribution within it. Preliminary results show that the cyclic loaded zone in the foil (plane stress) and in the Fe-3Si plate (plane strain) are essentially the same size as the corresponding "monotonic" zones. This result suggests that the cyclic flow stress at small strains is roughly 1/2 of the ordinary tensile yield stress consistent with the Bauschinger effect.
2. The observed similarities in the size, shape and strain distribution within the cyclic and monotonic zones lend support to the practice of adapting functional relations for the monotonic case to the fatigue problem. Estimates of the monotonic zone size and crack-tip displacement indicate that the material in front of a fatigue crack is subjected to about 50-150 cycles of reverse plastic deformation, of which about 2-7 cycles involve the large plastic strains experienced within the intensely deformed near-tip region. The crack advance per cycle is estimated to be 10-50% of the crack opening displacement.
3. The compilation of cyclic crack growth-rate measurements for steels, aluminum alloys and a titanium alloy provides evidence for 2 growth-rate regimes. Regime No. 1 involves the low stress intensity values and low growth rates usually $< 10^{-4}$ in. per cycle which correspond with the striation spacing, and a stress exponent $m \approx 2$. Regime No. 2 is the high stress-high growth rate portion of the spectrum usually $> 10^{-5}$ in. per cycle and a larger stress exponent, $m \geq 4$.
4. The cyclic crack growth resistance in Regime No. 1 is roughly proportional to the elastic modulus but relatively insensitive to yield strength, composition and ductility. Growth rate measurements on a variety of steels, aluminum alloys and Ti-6Al-4V can be approximated by the expression $\frac{da}{dN} \approx 8 \left(\frac{\Delta K}{E} \right)^2$, where E is the modulus. While neither the blunting or damage accumulation mechanisms easily account for all of the features of Regime No. 1, more of the existing observations can be rationalized by blunting.
5. Some of the features of Regime No. 2 can be explained by the mechanism responsible for Regime No. 1 together with the idea that crack growth is further enhanced by an increasing length of active crack front. This is thought to occur when the plastic zone is large enough to produce cracks at hard particles and other weak interfaces ahead of the main crack front which then also extend by cyclic growth and connect with the main crack. Accordingly, improvements in fatigue life could be realized by postponing the transition from Regime No. 1 to No. 2, and this may be related to metallurgical factors.

REFERENCES

- (1) Weibull, W., "The Propagation of Fatigue Cracks in Light-Alloy Plates", Svenska Aeroplan Aklieblaget, Linköping, SAAB TN 25 (January, 1954).
- (2) McEvily, A. J., and Illg, W., "The Rate of Crack Propagation in Two Aluminum Alloys", NACA TN 4394 (September, 1958).
- (3) Illg, W., and McEvily, A. J., Jr., "The Rate of Fatigue-Crack Propagation for Two Aluminum Alloys Under Completely Reversed Loading", NASA TN D-52 (October, 1959).
- (4) Donaldson, D. R., and Anderson, W. E., Proceedings of Crack Propagation Symposium, College of Aero, Cranfield, England, pp. 375-441 (September, 1961).
- (5) Hudson, C. M., and Hardrath, H. F., "Effects of Changing Stress Amplitude on the Rate of Fatigue Crack Propagation in Two Aluminum Alloys", NASA TN D-960 (September, 1961).
- (6) Broek, D., and Schijve, J., "The Influence of the Mean Stress on the Propagation of Fatigue Cracks in Aluminum Alloy Sheet", Nat. Aero. Res. Inst. (Amsterdam), Report NLR-TN M.2111 (January, 1963).
- (7) McEvily, A. J., Jr., Boettner, R. C., and Bond, A. P., "On Cold Work and Fatigue Crack Propagation in α -Brass, J. Inst. Met., 93, 481 (1964-65).
- (8) Carman, C. M., and Katlin, J. M., "Low Cycle Fatigue Crack Propagation of High Strength Steels", ASME 66-MET-3 (April, 1966).
- (9) Forman, R. G., Kearney, V. E., and Engle, R. M., "Numerical Analysis of Crack Propagation in Cyclic Loaded Structures", Trans. ASME, 89B (September, 1967).
- (10) Swanson, S. R., Cicci, F., and Hoppe, W., "Crack Propagation in Clad 7070-T6 Aluminum Alloy Sheet Under Constant and Random Amplitude Fatigue Loading", ASTM STP 415, p. 312, 1967.
- (11) Yokobori, T., Tanaka, M., Hayakawa, H., Yoshimura, and Sasakira, S., "Fatigue Crack Propagation Behavior of Mild Steel and High Strength Steels", Rep. of Res. Inst. Strength Fracture Matls. (Tohoku U.), 3, p. 39 (1967).
- (12) Wei, R. P., Talda, P. M., and Li, Che-Yi, "Fatigue Crack Propagation in Some High Strength Steels", ASTM Spec. Tech. Pub. No. 415, 460 (1967).
- (13) Crooker, T. W., Cooley, L. A., Lange, E. A., and Freed, C. N., "Subcritical Flaw Growth in 9Ni-4Co-0.25C Steel--A Fatigue and Fractographic Investigation and Its Relationship to Plane Strain Fracture Toughness", NRL Report 6698 (May, 1968).

- (14) Schwab, R. C., "The Use of Tapered Double-Cantilever-Beam Specimens for Fatigue-Crack Growth Studies", Navy Ship Res. Dev. Cent. Report No. 2689 (1968).
- (15) Bates, R. C., and Clark, W. G., Jr., "Fractography and Fracture Mechanics", Westinghouse Res. Lab. Report 68-1D7-RPAFC-P1 (September, 1968).
- (16) Crooker, T. W., and Lange, E. A., "Fatigue Crack Growth in Three 180-Ksi Yield Strength Steels in Air and in Saltwater Environments", NRL Report 6761 (September, 1968).
- (17) Hall, L. R., "Plane-Strain Cyclic Flaw Growth in 2014-T62 Aluminum and 6Al-4V (Zr) Titanium", NASA CR-72396 (November, 1968).
- (18) Miller, G. A., "The Dependence of Fatigue-Crack Growth Rate on Stress Intensity Factor and the Mechanical Properties of Some High Strength Steels", Trans. ASM, 61, 442 (1968).
- (19) Mowbray, D. F., Andrews, W. R., and Brothers, A. J., "Fatigue-Crack Growth-Rate Studies of Low-Alloy Pressure-Vessel Steels", ASME Paper No. 68 PVP-23 (1968).
- (20) Smith, S. H., Porter, T. R., and Sump, W. D., "Fatigue Crack-Propagation and Fracture-Toughness Characteristics of 7079 Aluminum Alloy Sheets and Plates in Three Aged Conditions", NASA CR-996 (1968).
- (21) Broek, D., "The Effect of Intermetallic Particles on Fatigue Crack Propagation in Aluminum Alloys", Proceedings 2nd International Conference on Fracture, Brighton, England (April, 1969).
- (22) Liu, H. W., and Iino, N., "A Mechanical Model for Fatigue Crack Propagation", Proceedings 2nd International Conference on Fracture, Brighton, England (April, 1969).
- (23) Barsom, J. M., "Investigation of Subcritical Crack Propagation", Thesis (U. of Pittsburgh), 1969.
- (24) Barsom, J. M., Inhot, E. J., and Rolfe, S. T., "Fatigue-Crack Propagation in High Yield-Strength Steels", J. Eng. Fract. Mech. (to be published).
- (25) Hudson, C. M. and Scardina, J. T., "Effect of Stress Ratio on Fatigue-Crack Growth in 7075-T6 Aluminum Alloy Sheet", Eng. Fract. Mech. (to be published).
- (26) Miller, G. A., "Fatigue Fracture Appearance and the Kinetics of Striation Formation in Some High Strength Steels", Trans. ASM (to be published).
- (27) Wei, R. P., and Landes, J. D., "The Effect of D₂O on Fatigue-Crack Propagation in a High Strength Aluminum Alloy", Int. J. Fract. Mech., 5, 69 (1969).
- (28) Rice, J. R., "Mechanics of Crack Tip Deformation and Extension by Fatigue", ASTM-STP 415, p. 247, (1967).

- (29) Rice, J. R., and Johnson, M. A., "The Role of Large Crack Tip Geometry Changes in Plane Strain Fracture", presented at the Battelle Colloquium on the Inelastic Behavior of Solids, Columbus and Atwood Lake, Ohio, September 15-19, 1969 (to be published).
- (30) Erdogan, F., "Crack-Propagation Theories", Fracture, Vol. 2, p. 497, Academic Press, New York, 1968.
- (31) Lehr, K. R., and Liu, H. W., "Fatigue Crack Propagation and Strain Cycling Properties", Int. J. Fract. Mech., 5, 45 (1969).
- (32) Felleux, R.M.N., "Mechanisms of Formation of Ductile Fatigue Striations", Trans. ASM, 62, 281 (1969).
- (33) Laird, C., "The Influence of Metallurgical Structure on the Mechanisms of Fatigue Crack Propagation", ASTM STP 415, p. 131, 1967.
- (34) McClintock, F. A., "On the Plasticity of the Growth of Fatigue Cracks", Fracture of Solids (Proceedings of the Maple Valley Fracture Conference), D. C. Drucker and J. J. Gilman, Ed., Interscience, New York, p. 65, (1963).
- (35) Manson, S. S., "Behavior of Materials Under Conditions of Thermal Strain", NACA TN 2933 (July, 1953).
- (36) Coffin, L. F., Jr., "A Study of the Effects of Cyclic Thermal Stresses in Ductile Metals", Trans. ASME, 76, 931 (1954).
- (37) Weertman, J., "Rate of Growth of Fatigue Cracks Calculated from the Theory of Infinitesimal Dislocations Distributed on a Plane", Int. J. Fracture Mech., 2, 460 (1966).
- (38) Weertman, J., "Growth of Fatigue Cracks Under Combined Static and Cyclic Stresses", Int. J. Fracture Mech., 5, 13 (1969).
- (39) Kanninen, M. F., Mukherjee, A. K., Rosenfield, A. R., and Hahn, G. T., "The Speed of Ductile-Crack Propagation and the Dynamics of Flow in Metals", U. S. Lindholm, Ed., Mechanical Behavior of Materials Under Dynamic Loads, Springer-Verlag, New York, 1968, p. 96.
- (40) Hahn, G. T., Kanninen, M. F., and Rosenfield, A. R., "Ductile Crack Extension and Propagation in Steel Foil", Proceedings 2nd International Conference on Fracture, Brighton, England (April, 1969).
- (41) Hahn, G.T., and Rosenfield, A. R., "Plastic Flow in the Locale of Notches and Cracks in Fe-3Si Steel Under Conditions Approaching Plane Strain", Ship Structure Committee Report SSC-191 (November, 1968).
- (42) Mostovoy, S., Crosley, P. B., and Ripling, E. T., "The Use of Crack-Line Loaded Specimens for Measuring Plane-Strain Fracture Toughness", J. of Materials, 2, 661 (1967).

- (43) Hahn, G. T., Rosenfield, A. R., and Sarrate, M., "Observations of Yielding Accompanying Crack Growth", presented at the Battelle Colloquium on the Inelastic Behavior of Solids, Columbus and Atwood Lake, Ohio, September 15-19, 1969 (to be published).
- (44) Tavernelli, J. F., and Coffin, L. F., Jr., "A Compilation and Interpretation of Cyclic Strain Fatigue Tests in Metals", Trans. ASM, 51, 438 (1959).
- (45) Fracture Strain Program Progress Letter to Ship Structure Committee (July 2, 1969).
- (46) Bilby, B. A., and Swinden, K.H., "Representation of Plasticity at Notches by Linear Dislocation Arrays", Proceeding, Royal Society of London, Vol. 285, p. 22, 1965.
- (47) Manson, S. S., "Fatigue: A Complex Subject-Some Simple Approximations", Exp. Mech., 5 (7), 193 (1965).
- (48) Laird, C., Private Communication.
- (49) McEvily, A. J., Jr., Boettner, R.C., and Johnston, T. L., "On the Formation and Growth of Fatigue Cracks in Polymers", Fatigue, An Interdisciplinary Approach, Sagamore Army Materials Research Conference Proceedings, Syracuse University Press 1964, p. 95.
- (50) McMillan, J. C., and Pelloux, R.M.N., "Fatigue Crack Propagation Under Program and Random Loads", Fatigue Crack Propagation, ASTM STP 415, 1967, p. 505.
- (51) Christensen, R.H., and Harmon, M. B., "Limitations of Fatigue-Crack Research in the Design of Flight Vehicle Structures", Fatigue Crack Propagation, ASTM STP 415, 1967, p. 5.
- (52) Hardrath, H. F., "Cumulative Damage", Fatigue, An Interdisciplinary Approach, Sagamore Army Materials Research Conference Proceedings, Syracuse University Press 1964, p. 345.
- (53) Erhardt, K., and Grant, N. J., "Behavior of 2024 Aluminum in Low Cycle Fatigue at Low Strain Rates as a Function of Temperature", Proceedings 2nd International Conference on Fracture, Brighton, England, 1969, Chapman and Hall, p. 702.
- (54) Hoepfner, D. W., "The Effect of Grain Size on Fatigue Crack Propagation in Copper", ASTM STP 415, p. 486, 1967.
- (55) Liu, H. W., "Fatigue Crack Propagation and the Stresses and Strains in the Vicinity of a Crack", App. Mat. Res., 7, 229 (1964).
- (56) Johnson, H. H., and Paris, P. C., "Sub-Critical Flaw Growth", Eng'g. Fracture Mech., 1, 3 (1969).

- (57) Hahn, G. T., and Rosenfield, A. R., "Local Yielding and Extension of a Crack Under Plane Stress", Acta Met., 13, 293 (1965).
- (58) Rosenfield, A. R., Dai, P. K., and Hahn, G. T., "Crack Extension and Propagation Under Plane Stress", Proceedings of the First International Conference on Fracture (1965), Vol. 1, pp. 223-258.

APPENDIX A--Compilation of Cyclic Crack-Growth Rate Measurements

Noticeable departures from a simple exponential crack growth relation $\frac{da}{dN} = A(\Delta K)^m$ were noted by Liu⁽⁵⁵⁾ as early as 1964. In the interim, most workers have tended to gloss over irregularities and have attributed a single mechanism, $m \sim 4$ to the entire growth rate spectrum⁽⁵⁶⁾. However, the recent work of Bates and Clark⁽¹⁵⁾, Barsom, et al.⁽²⁴⁾ and measurements of the stress dependence of the striation spacing^(15,21,26) offer good evidence for two regimes of the behavior:

Regime No. 1. This is the low stress-low growth rate portion of the spectrum, e.g., usually less than 10^{-4} in. per cycle, where the macroscopic growth rate coincides with the striation spacing^(15,21,26). As shown in Tables A-1 and 4, growth rates for a wide range of alloys are approximately described by the following empirical expression:

$$\frac{da}{dN} \approx A' \left(\frac{\Delta K}{E} \right)^2 \quad (A-1)$$

where $A' \sim 8$.

Regime No. 2. This is the high stress-high growth rate position of the spectrum, e.g., usually more than 10^{-5} in. per cycle. In this range growth rates tend to exceed the striation spacing and displays a greater stress sensitivity, e.g., $m \gtrsim 4$.

These two regimes are shown schematically in Figure A-1 which also defines the symbols used here to characterize the two regimes and the transition. The compilation of crack growth rate measurements in Table A-1 represents a conscious effort to identify two types of behavior and to assign them to Regimes No. 1 and No. 2 on the basis of the exponent. In some cases, neither a clear-cut change in behavior nor a characteristic m could be detected, and the Regime assignment is arbitrary. The compilation is mainly for growth rate measurements in air, with $R \sim 0$, but Barsom's⁽²³⁾ measurements for 12Ni-5Cr-3Mo Steel in NaCl and Wei and Landes⁽²⁷⁾ results for 7075-T651 in Argon and H₂O are included to illustrate the potency of "aggressive" environments.

It should be noted that when the coefficient A is evaluated empirically, it involves the exponent m : $A \equiv \left(\frac{da}{dN} \right)_i \Delta K_i^{-m}$ (where $\left(\frac{da}{dN} \right)_i$ is the growth rate corresponding to ΔK_i). Since m is frequently not known with precision, uncertainties in m are magnified in A even where ΔK_i is established accurately. For this reason ΔK_i is a more reliable index of performance than A , and ΔK_i and m (rather than A and m) are used here to characterize the growth rates and for purposes of comparison.

TABLE A-1. SUMMARY OF CYCLIC CRACK GROWTH DATA

| Material | Regime No. 1 | | | Transition | | Regime No. 2 | | | References |
|-----------------------------|--------------|---------------------------|--------------------------------|------------------|-------------------------------|--------------|---------------------------|--------------------------------|---|
| | Y (ksi) | ΔK-DATA RANGE (ksi√in) | ΔK ₁₀₋₅ (ksi√in) | m | ΔK ₁₋₂ (ksi√in) | Y (√in) | ΔK-DATA RANGE (ksi√in) | ΔK ₁₀₋₃ (ksi√in) | |
| | | | | | | | | | |
| Part I. Steels | | | | | | | | | |
| A508-351 (c) | 54 | - | 38 | - | - | - | - | ~165 | Present Study (19) |
| A-302B (d) | 59 | - | - | - | - | - | - | ~130 | Hobray, et al |
| A-302B (e) | 51 | - | - | - | ~40 | ~0.8 | - | ~200 | " |
| A-508-2 (d) | 65 | - | - | - | - | - | - | ~150 | Bates and Clark (15) |
| A-508-2 (e) | 67 | - | - | - | - | - | - | - | " |
| A-533 | 73 | 30-100 (e) | 38/40 (e) | 2.1/2.2 (e) | - | - | - | - | Barsom, et al (14) |
| 3Ni-Mo-V | 93 | 30-150 | 34 | ~1.85 | - | - | - | - | " |
| HY-80 (a) | 81 | 21-61 | 38 | 2.48 | - | - | - | - | Yokobori, et al (11) |
| HY-80 (b) | 93 | 23-50 | 33 | 2.34 | - | - | - | - | Barsom, et al (14) |
| HY-100 Steel | 109 | 5.6-26 | 20/23 | 2.3/2.6 | - | - | - | - | " |
| HY-130 (a) | 139 | 19-68 | 28 | 2.16 | - | - | - | - | " |
| HY-130 (b) | 140 | 42-92 | 29.5 | 2.13 | 92 | 0.66 | 92-150 | 140 | " |
| 4340 (ANNEALED) | 60 | 14-20/25 | 20 | 2.2/2.6 | 20/25 | 0.3/0.4 | 20/25-35 | ~120 | Liu and Ting (21) |
| 4340 (Q & T @ 1400F) | 63 | - | 35 | - | - | - | 25-70 | 4.0 | Miller (18,26) |
| 4340 (Q & T @ 1000F) | 163 | 20-80 | 33 | 2.4/2.26 (e) | ~80 | 0.49 | 80-110 | ~120 | " |
| 4340 (Q & T @ 500F) | 221 | 20-80 | 33 | 2.6 | ~80 | 0.36 | 80-90 | ~95 | " |
| 4340 (Q & T @ 200F) | 193 | - | - | - | - | - | 20-45 | ~50 | " |
| 9Ni-4Co-0.25C | 180 | - | - | - | - | - | 40-100 | 90 | Crooker, et al (13) |
| 9Ni-4Co-0.25C (a) | 175/180 | 45-80 | ~34 | ~1.85 | - | - | - | ~165 | Bates and Clark (15) |
| 10Ni-Cr-Mo-Co (a) | 191 | 5.5-86 | 35 | 2.25 | 86 | 0.45 | 86-140 | ~165 | Barsom, et al (14) |
| 10Ni-Cr-Mo-Co (b) | 182 | 30-60 | 30 | 2.24 | - | - | - | - | " |
| 12Ni-5Cr-3Mo (a) | 185 | 21-60 | 31 | 2.16 | - | - | - | - | " |
| 12Ni-5Cr-3Mo (b) | 184 | 25-60 | 28 | 2.18 | - | - | - | - | " |
| 12Ni-5Cr-3Mo | 194 | 33-80 | 33 | 2.3 | 80 | - | 80-105 | ~130 | Schwab (14) |
| 12Ni-5Cr-3Mo (NaCl, 600CPM) | 184 | 15-53 | 26 | ~2.0 | - | - | - | ~5.0 | Barsom (22) |
| 12Ni-5Cr-3Mo (NaCl, 60CPM) | 184 | 18-55 | 23 | ~2.0 | - | - | - | - | " |
| 12Ni-5Cr-3Mo (NaCl, 6CPM) | 184 | 20-47 | 16 | ~2.0 | - | - | - | - | " |
| 12Ni-Mnaging | 180 | 25-100 | 25 | 2.3 | - | - | - | - | Crooker and Lange (16) |
| 18Ni-Mnaging | 180 | 42-90 | ~16 | 2.3 | - | - | - | - | " |
| 18Ni-Mnaging | 218 | 20-80 | 31 | 2.3/2.5/1.42 (e) | ~80 | - | 80-100 | ~110 | Miller (18,26) |
| 18Ni-Mnaging | 245 | 20-100 | 35 | 2.88/1.74 (e) | - | - | - | ~150 | " |
| 18Ni-Mnaging | 246/252 | 20-80 | 36 | 2.4 | 80 | 0.32 | 80-100 | - | Wei, et al (12) and Carman and Katlin (8) |
| 18Ni-Mnaging | 295/308 | 18-60 | 35 | 2.6 | - | - | - | - | Wei, et al (12) and Carman and Katlin (8) |
| H 11 | 208 | - | - | - | - | - | - | - | Carman and Katlin (8) |
| H 11 | 242 | - | 34 | - | - | - | 21-29 | ~50 | Miller (18,26) |
| D6AC | 241 | 32-80 | 12 | ~2.8 | ~70 | - | 27-60 | ~120 | Carman and Katlin (8) |

(a) 1-in.-thick plate
 (b) 2-in.-thick plate
 (c) Thickness direction
 (d) Axial direction
 (e) Based on striation spacing

TABLE A-1. SUMMARY OF CYCLIC CRACK GROWTH DATA (CONTINUED)

| Material | Regime No. 1 | | | Transition | | Regime No. 2 | | | References | |
|------------------------------|--------------|--------------------------------|----------|-------------------------------|---------------------------|--------------------------------|-----------------|--------------------------------|------------|---|
| | Y (Ksi) | ΔK-DATA RANGE (Ksi√In) | | ΔK ₁₋₂ (Ksi√In) | ΔK ₁₀ (√In) | ΔK-DATA RANGE (Ksi√In) | | ΔK ₁₀₋₃ (Ksi√In) | | |
| | | ΔK ₁₀₋₅ (Ksi√In) | m | | | ΔK ₁₀₋₃ (Ksi√In) | m | | | |
| Part 2. Aluminum Alloys | | | | | | | | | | |
| 7075-T6 | 70 | 5-22 | 7.5 | 2.3 | 22 | 0.31 | 22-42 | 30 | ~ 5.5 | Forman, et al (9) and McEvily and Illig (2) |
| 7075-T6 | 70 | 6-24 | 10 | 2.4 | 24 | 0.34 | 24-65 | 40 | ~ 5.7 | Forman, et al (9) and Hudson and Hardrath (5) |
| 7075-T6 (R = 0.3) | 70 | 5-18 | 8 | 2.8 | 18 | 0.25 | 18-22 | - | - | Forman, et al (9) and Broek and Schijve (6) |
| 7075-T6 | 73.5 | 6-11 | 6 | 2.75 | 13 | - | 13-30 | ~ 22 | ~ 5 | Hudson and Scardina (25) |
| 7075-T651 (Argon) | 70 | 5-20 | 10 | 2/2 (o) | 20 | - | 20-28 | ~ 33 | ~ 6 | Broek (21) |
| 7075-T651 (H ₂ O) | 70 | 9-22 | 14.5 | 3.6 | - | - | - | - | - | Wei and Landes (27) |
| 2024-T3 | 50 | 6-18 | 8 | 3.6 | - | - | - | - | - | " |
| | | 7-29 | 9.5/13 | 2.6/3 | 29 | 0.58 | 29-70 | 40 | ~ 6.8 | Donaldson and Anderson (4) |
| 2024-T3 (R = -1) | 50 | 5-22 (a) | 10.5 (a) | 2.9 | 22 (a) | 0.44 (a) | 22 (a) - 25 (a) | ~ 33 (a) | - | McEvily and Illig (2) |
| 2024-T3 (R = 0.3) | 50 | 4-10 | 8 | 3 | 18 | 0.36 | 18-22 | 24 | - | Hudson and Hardrath (5) |
| 2024-T3 (R = 0.25) | 50 | 6-16 | 10.5 | 4.9 | 16 | 0.32 | 16-40 | 35 | ~ 4.5 | Weiull (1) |
| 2024-T351 | 50 | 4-12 | 6 | 2.6 | 12 | 0.24 | 12-20 | ~ 4 | - | Forman, et al (9) |
| 2024-T3 | 50 | 5-26 | 14 | 2.5/2 (b) | - | - | 26-33 | ~ 38 | ~ 10 | Broek and Schijve (6) |
| 7079-T6 | 65 | 8-30 | 12 | 2.6/2.1 (b) | - | - | - | - | - | Liu and Jino (22) |
| 7079-T6 | 68 | 6-13 | ~ 7 | 2.7 | 13 | 0.19 | 13-20 | ~ 20 | ~ 7 | Broek (21) |
| 7079-T6 | 70 | 15-50 | 10/15 | ~ 3 | - | - | - | - | - | Bates and Clark (15) |
| 5456-H321 | 37 | 9-20 | 12 | 2.1/2.1 | - | - | - | - | - | Swanson, et al (10) |
| | | | | | | | | | | Smith, et al (20) |
| | | | | | | | | | | Bates and Clark (15) |
| Part 3. Titanium Alloys | | | | | | | | | | |
| Ti-6Al-4V | 127 | 13-35 | 15 | 3/2 (b) | - | - | - | - | - | Bates and Clark (15) |
| Ti-6Al-4V | 121 | 40-66 | 38 | ~ 4 | - | - | - | - | - | Hall (17) |
| Part 4. Miscellaneous Alloys | | | | | | | | | | |
| 70-30 Brass (Annealed) | 18 | | 14 | ~ 5 | | | | | | McEvily, et al (7) |
| 70-30 Brass (cold worked) | 92 | | 14 | ~ 5 | | | | | | " |

(a) Values quoted represent 1/2 the value reported because R = 1

(b) Based on striation spacing

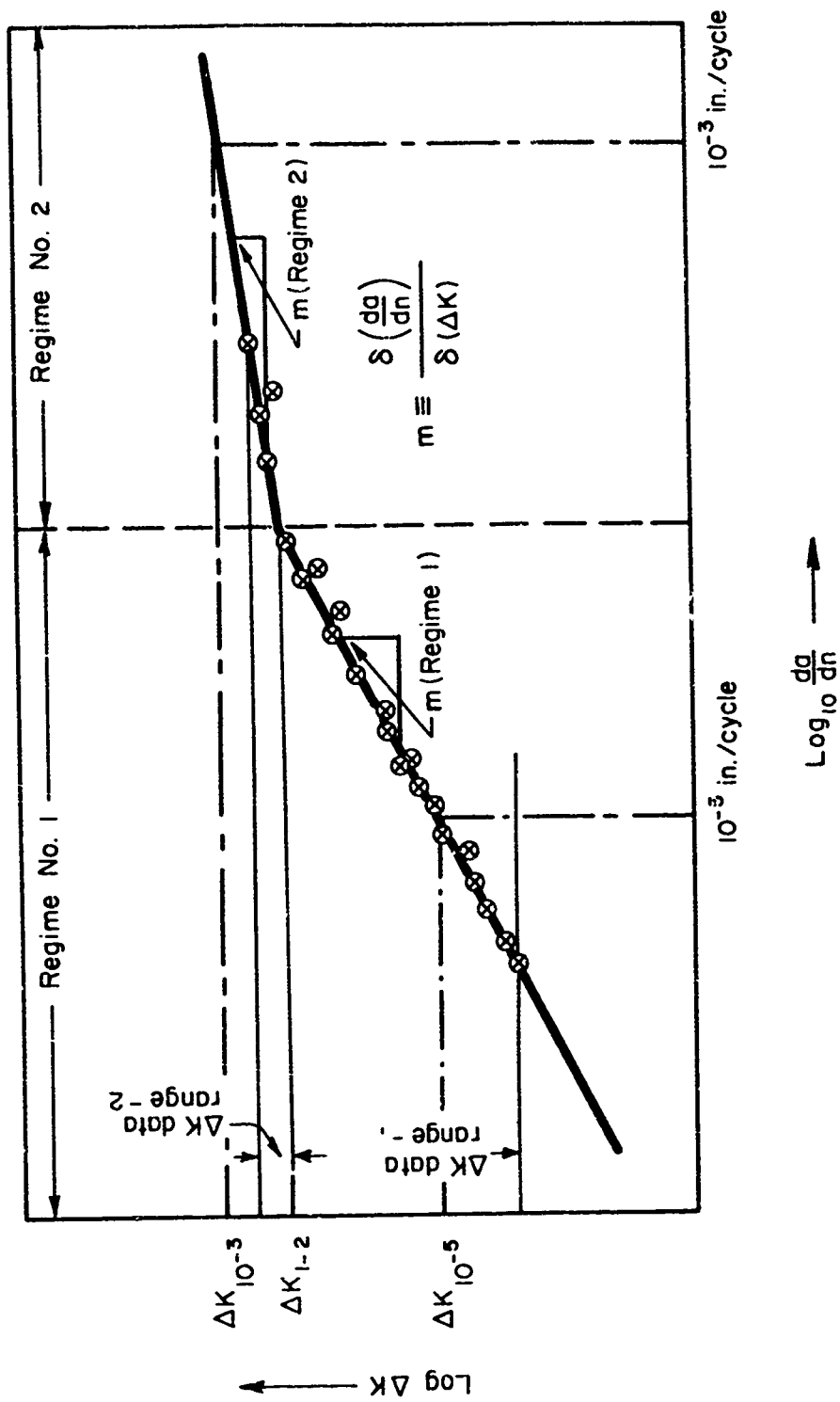


FIGURE A-1. SCHEMATIC OF STRESS-INTENSITY-GROWTH RATE SPECTRUM WITH 2 REGIMES AND DEFINITIONS OF TERMS IN TABLE A-1

APPENDIX B--Simplified Formulations of the Cyclic Crack Growth Mechanisms

A. Irreversible Plastic Blunting. This process can be formulated approximately by noting that $\frac{da}{dN}$, the crack advance per cycle will be a fraction β of the COD (Equation 4B):

$$\frac{da}{dN} = \beta \cdot COD \approx \beta \cdot \frac{\Delta K^2}{4EY_c} \quad (B-1)$$

where β , the efficiency (or degree of irreversibility) of the blunting process is regarded as constant to a first approximation.

B. Damage Accumulation. This mechanism is described in essentially the same way as proposed by Lehr and Liu⁽³¹⁾ by combining Equations 5 and 6 with the Manson-Coffin fatigue damaged law^(35,36,47):

$$n^{1/2} \Delta \epsilon_p^- = B \quad (B-2)$$

where $\Delta \epsilon_p^-$ is regarded as the weighted average plastic strain range and B the fracture strain for monotonic loading: This gives two results:

$$\text{small strain} \quad \frac{da}{dN} \approx \frac{0.03 \Delta \epsilon_p^- \Delta K^2}{4B^2 Y_c^2} \sim \frac{0.1}{B^2} \left(\frac{\Delta K}{E} \right)^2 \quad (B-3)$$

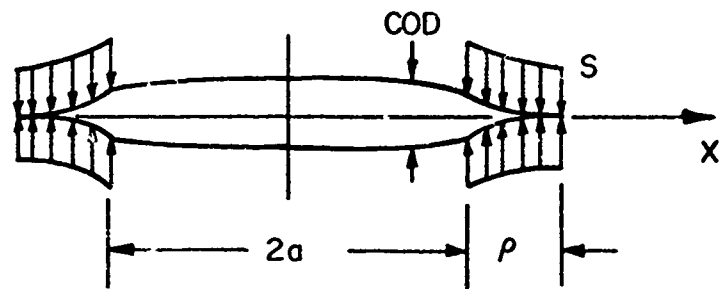
$$\text{large strain} \quad \frac{da}{dN} \approx \frac{\Delta \epsilon_p^{-2} \Delta K^2}{4B^2 E Y_c} \quad (B-4)$$

In the first, $\Delta \epsilon_p^{-2}$ is the strain range averaged over all cycles, which Liu and Liu estimate as $\Delta \epsilon_p^- \approx 4 \frac{Y_c}{E}$ and is consequently a relatively small strain, e.g., $\Delta \epsilon_p^- \approx 0.02$. In the second, only the number of cycles involving large strains is considered and $\Delta \epsilon_p^- \sim 0.5$ ⁽²⁹⁾.

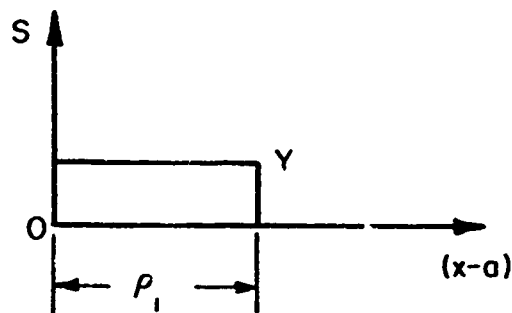
APPENDIX C--Augmented Dugdale Model

At the tip of a fatigue crack there exists a very heavily strained region where Y_c , the cyclic yield stress, may be greatly in excess of Y , the yield stress for ordinary monotonic loading. Simultaneously, Y_c may be less than Y in the remaining, lightly strained region of the plastic zone as a result of the Bauschinger effect. A model of this behavior is given in Figure C-1. Figure C-1a shows the Dugdale Model with the tips of the crack being pressed together by a traction denoted S . The region $-a < x < a$ represents the crack, $a < x < a + \rho$ the plastic zone. Usually S is set equal to a constant yield stress as in Figure C-1b. For the case of the fatigue crack, the distribution shown in Figure C-1c is postulated.

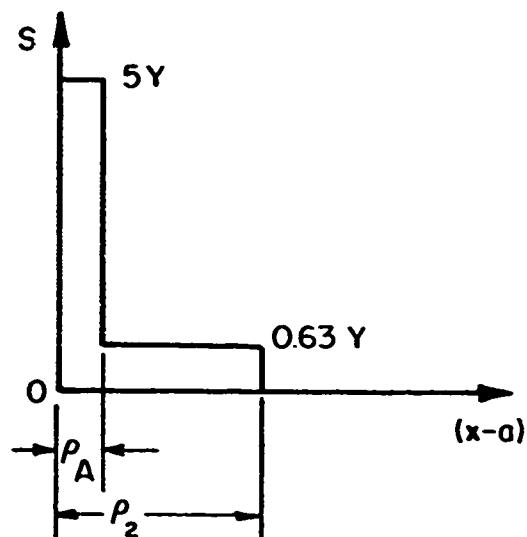
The two Y_c -levels represent the small heavily strained region where $Y_c = 5Y$ and the lightly strained region where $Y_c = 0.63Y$. According to the calculation, which was made by methods outlined in References (57) and (58), COD (Case 2) = $1/5$ COD (Case 1), when $\rho_1 = \rho_2$, $\rho_2/\rho_A = 5.5$ and $\frac{T}{Y} = 0.25$, where T is the nominal applied stress. Thus, there is a large difference in COD even though the plastic zones are the same size. Also the COD for the fatigue crack model is comparable to a much stronger material even though the heavily strained region occupies a small part of the total plastic zone. The model illustrates that the COD is strongly influenced by the value of Y appropriate for material closest to the crack tip.



a. Dugdale Model



b. Case 1 - Constant Flow Stress



c. Case 2 - Model of Flow Stress Distribution for Fatigue Crack

FIGURE C-1. AUGMENTED DUGDALE CRACK MODEL

UNCLASSIFIED

Security Classification

| DOCUMENT CONTROL DATA - R & D | | |
|--|------------------------------|--|
| (Security classification of title body of abstract and indexing annotation must be entered when the overall report is classified) | | |
| 1. ORIGINATING ACTIVITY (Corporate author) Battelle Memorial Institute Columbus Laboratories 505 King Avenue Columbus, Ohio 43201 | | 2a. REPORT SECURITY CLASSIFICATION Unclassified |
| 3. REPORT TITLE ELASTIC-PLASTIC FRACTURE MECHANICS | | 2b. GROUP |
| 4. DESCRIPTIVE NOTES (Type of report and inclusive dates) Final Report - April 1, 1968 to September 30, 1969 | | |
| 5. AUTHOR(S) (First name, middle initial, last name) G. T. Hahn, A. R. Rosenfield, and M. Sarrate | | |
| 6. REPORT DATE January 1970 | 7a. TOTAL NO. OF PAGES 49 | 7b. NO. OF REFS 53 |
| 8a. CONTRACT OR GRANT NO. AF 33(615)-3565 | | 9a. ORIGINATOR'S REPORT NUMBER(S) |
| b. PROJECT NO. 7351 | | 9b. OTHER REPORT NO(S) (Any other numbers that may be assigned this report) AFML-TR-67-143, Part III, Final Report |
| c. TASK NO. 735106 | | |
| d. | | |
| 10. DISTRIBUTION STATEMENT This document is subject to special export controls and each transmittal to foreign governments or foreign nationals may be made only with prior approval of the Metals and Ceramics Division (MAM), Air Force Materials Laboratory, Wright-Patterson Air Force Base, Ohio 45433. | | |
| 11. SUPPLEMENTARY NOTES | | 12. SPONSORING MILITARY ACTIVITY Metals and Ceramics Division (MAM) Air Force Materials Laboratory Wright-Patterson AFB, Ohio 45433 |
| <p>13. ABSTRACT This report describes experiments that delineate the plastic zone of a growing fatigue crack and its relation to the zone of a monotonically loaded, stationary crack. A compilation of cyclic crack growth measurements is also presented. Preliminary results of the zone studies and the data compilation are examined with respect to the mechanism of cyclic growth and the contribution of metallurgical factors.</p> <p>Two techniques, etch pitting and interferometry, are used to reveal the plastic zones produced by growing fatigue cracks in Fe-3Si Steel (under plane strain) and in cold worked steel (under plane stress), respectively. In addition, a method of simulating cyclic crack growth under controlled conditions by cutting-in slits under load with intermittent load reversals is demonstrated. The preliminary results indicate that the plastic deformation generated by each loading cycle is similar to the deformation of the monotonic zone.</p> <p>The results provide a basis for extending numerical treatments of the monotonically loaded crack to the fatigue crack problem. Estimates are made in this way of the number of plastic strain cycles experienced by the material in front of a growing fatigue crack and also the crack-tip displacement. The values obtained lend support to Lehr and Liu's treatment of cyclic crack growth which is based on Manson-Coffin type damage accumulation. Their analysis is in good accord with measurements of the cyclic cracking resistance and fatigue striation spacing observed in Regime No. 1--the low stress sensitive, low growth rate portion of the spectrum. A possible explanation for the greater stress sensitivity and higher growth rates in Regime No. 2 is offered in terms of an increasing length of active crack front.</p> <p>Both the theoretical treatment and the bulk of the test data show that the resistance to fatigue crack growth in Regime No. 1 is relatively insensitive to composition and metallurgical structure, provided environmental effects are not involved. In contrast, significant improvements in fatigue life could be achieved simply by postponing the onset of Regime No. 2, a feature that should depend on metallurgical variables.</p> | | |

DD FORM 1 NOV 65 1473

(Unclassified)

Security Classification

Unclassified

Security Classification

| 14 | KEY WORDS | LINK A | | LINK B | | LINK C | |
|----|---|--------|----|--------|----|--------|----|
| | | ROLE | WT | ROLE | WT | ROLE | WT |
| | Cyclic Crack Growth Fatigue Fracture Mechanics Plastic Zones at Crack Tips Stable Crack Growth High-Strength Steels High-Strength Aluminum Alloys High-Strength Titanium Alloys Non-Uniform Loading Finite Plate Effects Elastic-Plastic Analysis | | | | | | |

Unclassified

Security Classification